CDH18 is a fetal epicardial biomarker regulating differentiation towards vascular smooth muscle cells

（CDH18 は血管平滑筋細胞への分化を制御する胎児心外膜バイオマーカーである）

Junghof Julia

CDH18 is a fetal epicardial biomarker regulating differentiation towards vascular smooth muscle cells

Julia Junghof[1,2], Yuta Kogure[1,3], Yu Tian[1,2], Eva María Verdugo-Sivianes[4,5], Megumi Narita[1], Antonio Lucena-Cacace[1 *], and Yoshinori Yoshida[1 *]

[1] Center for iPS Cell Research and Application, Department of Cell Growth and Differentiation, Kyoto University, Kyoto, Kyoto 606-8507, Japan

[2] Graduate School of Medicine, Kyoto University, Kyoto, Kyoto 606-8501, Japan.

[3] Research and Development Division, ROHTO Pharmaceutical Co., Ltd., Osaka, Osaka 544-8666, Japan.

[4] Instituto de Biomedicina de Sevilla, IBIS, Hospital Universitario Virgen del Rocío, Universidad de Sevilla, Consejo Superior de Investigaciones Científicas, Avda. Manuel Siurot s/n, 41013 Seville, Seville, Spain.

[5] CIBERONC, Instituto de Salud Carlos III, 28029 Madrid, Madrid, Spain.

* Co-correspondence: Yoshinori Yoshida (Y.Y.), Antonio Lucena-Cacace (A.L-C.)

yoshinor@cira.kyoto-u.ac.jp, telephone: (+81) 075-366-7371

a.lucena@cira.kyoto-u.ac.jp telephone: (+81) 080-7894-0095

ABSTRACT

The epicardium is a mesothelial layer covering the myocardium serving as a progenitor source during cardiac development. The epicardium reactivates upon cardiac injury supporting cardiac repair and regeneration. Fine-tuned balanced signaling regulates cell plasticity and cell-fate decisions of epicardial-derived cells (EPCDs) via epicardial-to-mesenchymal transition (EMT). However, powerful tools to investigate epicardial function, including markers with pivotal roles in developmental signaling, are still lacking. Here, we recapitulated epicardiogenesis using human induced pluripotent stem cells (hiPSCs) and identified type II classical cadherin CDH18 as a biomarker defining lineage specification in human active epicardium. The loss of CDH18 led to the onset of EMT and specific differentiation towards cardiac smooth muscle cells. Furthermore, *GATA4* regulated epicardial *CDH18* expression. These results highlight the importance of tracing *CDH18* expression in hiPSC-derived epicardial cells, providing a model for investigating epicardial function in human development and disease and enabling new possibilities for regenerative medicine.

KEYWORDS

epicardium, epicardiogenesis, epicardial development, CDH18, EPDCs, EMT, SMC, CF, WT1, hiPSC-derived epicardial cells, epicardial activation

INTRODUCTION

Cardiovascular diseases are the leading cause of death worldwide. The human heart is incapable of restoring itself and myocardial repair and regeneration processes are still poorly understood. In recent years the epicardium has emerged as a therapeutic target, given its ability to re-activate upon cardiac injury and promoting cardiac repair [1]. The epicardium is a mesothelial layer covering the myocardium and serves as a progenitor source supporting cardiac development, repair and regeneration [2-4]. Epicardiogenesis is evolutionary conserved and absolutely essential for cardiac development, with failure of epicardial formation being embryonic lethal [5, 6]. After formation of the proepicardium (PE), a transient cauliflower-like structure at the venous pole of the looping heart, cells of the PE migrate over and cover the looping heart tube completely, subsequently forming the epicardium. The embryonic epicardium is active, epicardial cells are proliferative and have the ability to undergo epicardial epithelial-to-mesenchymal transition (EMT). Those epicardial-derived cells (EPDCs) can proliferate and migrate, invading the underlying myocardium, where they subsequently differentiate into various cardiac cell types like vascular smooth muscle cells (SMC), cardiac fibroblasts (CF) and, to a lesser degree, endothelial cells (EC) [7-9]. The epicardium and EPDCs exhibit extensive developmental plasticity, which is crucial for cardiogenesis, by contributing to coronary vessel formation as well as myocardial growth and maturation [1, 2, 4, 10, 11]. During adulthood, the epicardium enters quiescence and serves as a protective layer. Only upon cardiac injury, the epicardium re-activates and contributes as a quick transient progenitor hub of derivative cells to the cardiovascular system regeneration [4, 12]. This fact provides the epicardium with a pivotal role mediating regenerative responses. Unlike other species, mammals lack the ability to restore the heart. Nonetheless, re-activation of the epicardium is required for cardiac scar formation as well as coronary vessel growth[13]. Not only promotes the epicardium myocardial regeneration via paracrine signaling, it also mediate inflammatory responses[14, 15]. Moreover, engineered patches carrying epicardial follistatin-like 1 (FSTL-1) were able to enhance cardiac regenerative responses[16]. However, despite ongoing investigation on the epicardium as a therapeutic target tissue, processes governing epicardial development, re-activation and engraftment ability are not well understood, mainly due to lacking comprehension of the fundamental biology behind the epicardium

itself, including the expression dynamics of epicardial epitopes mediating tissue responses to homeostasis disruptions and cellular signaling upon cardiac damage.

The epicardium coordinates a complex network of surface remodelers in order to respond to different stimuli driven by organ development and tissue repair [11, 17]. The cell surfaceome describes the whole proteome of surface and transmembrane proteins. During tissue morphogenesis, homeostasis and regeneration, the surfaceome, particularly surface remodelers, plays an essential role in expansion, migration and invasion, forming complex cellular structures [18]. However, cell-surface markers defining functional epicardial cells or regulating epicardial cell-fate decisions have been difficult to identify.

The cadherin family of cell-cell adhesion proteins are important for tissue morphogenesis [19]. Even though cadherins may have originated to facilitate mechanical cell-cell adhesion, their functions are pleiotropic and have evolved to be imperative for many other aspects, including cell recognition, coordinated cell movements, cell-fate decisions and the maintenance of structural tissue polarity, by controlling diverse signaling pathways [20-25].

In this study, we identified type II classical cadherin CDH18, formerly known as cadherin 14 (CDH14), as a specific biomarker expressed in fetal-stage epicardium, defining cellular specification. Human pluripotent stem cells (hPSCs) [26, 27] and their capacity to differentiate into cardiac cells allow recapitulation of epicardiogenesis *in vitro* [28-36]. Here we generated human induced (hi)PSC-derived epicardial-like (EPI) cells. Epicardial identity was associated with sustained expression levels of key epicardial genes and retained *CDH18* expression in correlation to *GATA4* expression, an essential transcription factor proven to be required to form proepicardium *in vivo* [37]. The loss of *CDH18* expression led to the activation of cell-fate specific EMT towards SMC differentiation, confirming an important biological function of *CDH18*, not only to define progressive epicardial lineage specification, but also to regulate downstream signaling that drives EPDC derivation. Our study sets a basis for a reproducible model to investigate epicardial function in human cardiac development and disease, ultimately enabling new possibilities in regenerative medicine.

RESULTS

Defined transcriptome of developing epicardial surfaceome revealed the enrichment of *CD22* and *CDH18* in late-stage populations

To investigate the expression profiles of the epicardium, we compared RNA-Seq dataset of induced epicardial-like cells at day (d) 12 (Epi12) and 48 (Epi48) representing a developmental early- and late-stage respectively and investigated their relationship with the adult quiescent epicardium [28]. Whole mRNA transcriptome-based principal-component analysis (PCA) demonstrated 84.75% variance between Epi12 and Epi48 populations (Figure 1a), with the biggest difference observed between Epi12 and adult - quiescent - cells (Supplementary Figure 1a-b). The active embryonic epicardium is defined by the expression of the transcription factors Wilms' tumor 1 (*WT1*) and T-Box 18 (*TBX18*), followed by aldehyde dehydrogenase 1 member A2 (*ALDH1A2*), distinguishing it from the myocardium and endocardium, as well as the adult epicardium which lies quiescent (Supplementary Figure 1c). All three genes were upregulated in correlation to each other over time (Supplementary Figure 1d-e), confirming the embryonic epicardial identity of the transcriptome profiles. Comparative analysis of genes in correlation to *WT1, TBX18 and ALDH1A2*, unveiled 2221 common genes in their intersection (Figure 1b), with 49 genes identified as surface protein encoding. We also found 825 differentially expressed genes (DEGs) between Epi12 and Epi48 populations (Supplementary Figure 1f) allowing us to subsequently define a putative transcriptome of epitopes of the active epicardium (Figure 1c).

Next, we excluded genes that had no significant negative correlation to the endothelial cell markers *CDH5* and *PECAM1* (Figure 1d) and selected late-stage upregulated genes (Figure 1e) that showed highly positive correlation to epicardial genes (Figure 1f), obtaining *CD22* and *CDH18* as candidate cell surface biomarkers in active epicardium. We then confirmed that both candidates were not longer expressed in adult tissue similar to active epicardial key genes (Figure 1g and Supplementary Figure 1g). Next, we verified their absence in two important epicardial derivatives. While CF and SMC markers were upregulated in their respective cellular identities, no mRNA expression of *CD22* or *CDH18* was detected (Figure 1h-i). Moreover, we confirmed tissue specificity using independent

datasets: Heart *CD22* expression ranked #2 after central nervous system (CNS), and heart *CDH18* expression ranked #3 after CNS and testis (Supplementary Figure 1h), two known CDH18-expressing tissues [38-40]. Finally, as an increase of CDH18 is difficult to observe during heart development of mouse embryos due to cellular heterogeneity in the bulk population (Supplementary Figure 1i), we organotypically cultured explanted epicardial tissue from E14 hearts and documented CDH18 expression in epicardial explants (Supplementary Figure 1i). We confirmed the epicardial specificity of CDH18 expression in a physiological context of cardiac cells derived from human embryos ranging different time points of gestation (Figure 1j-k).

CDH18 but not CD22 is an epicardial biomarker defining progressive lineage specification

To define the expression pattern of *CD22* and *CDH18*, we first recapitulated epicardiogenesis *in vitro*. We modified previously reported induction methods for hiPSC-derived epicardial-like (EPI) cells [28, 32, 35] to robustly yield $WT1^+$ cells at a higher rate, and long-term culture of cells was achieved by permanent inhibition of transforming growth factor (TGF)-β (Figure 2a). As epicardial cells and atrial cardiomyocytes share a common progenitor pool during development [3], we excluded the presence of any residual myocyte traces in our system, by generating EPI cells from MYH6 reporter line (MYH6-EIP4) [41], obtaining no cardiomyocytes (Supplementary Figure 2a-c). Moreover, absence of endothelial markers CD31 and CD144 ensured that no cells of endothelial nature were present (Supplementary Figure 2d-f). EPI cells showed typical epicardial cobblestone-like morphology (Figure 2b), and key active epicardial genes (*WT1* and *TBX18)* started to be upregulated as early as d12 continuing so until d24 (Figure 2c). In agreement with previous models, cells did not upregulate *ALDH1A2* - a gene highly expressed in the epicardium but not PE - until d24, indicating that the cells at d12 represented an early stage during development comparable to PE cells and specified into later stage epicardium at d24 (fetal-like) (Figure 2c-d). We found all genes expressed in correlation to each other (Supplementary Figure 3a), and did not observe significant differences in their expressions after d24 (Supplementary Figure 3b-c), endorsing that cells had

completed differentiation into fetal-stage epicardium by d24. We also confirmed WT1 protein expression on this day by immunofluorescence (Supplementary Figure 3d-f).

We then checked *CD22* expression levels during epicardial differentiation. We found *CD22* expression increased but failed to detect CD22 protein in d24 EPI cells, suggesting protein translation insufficiency, and therefore invalidating CD22 as a suitable biomarker (Supplementary Figure 4).

Next, we investigated *CDH18* levels and could verify its expression in EPI cells derived from different hiPSC lines (Figure 2f and Supplementary Figure 5a). Both mRNA and protein (Figure 2e-g) levels increased exponentially over time of epicardial differentiation and CDH18 was co-expressed with WT1 in a highly correlated fashion (Figure 2g-h and Supplementary Figure 5), implying a potential role during epicardial specification.

Epicardial cells have the potential to transit into EPDCs via EMT and subsequently differentiate into CF and SMC during development and also after re-activation upon cardiac injury. This functionality has also been well reported *in vitro* by treatment with basic fibroblast growth factor (bFGF) and TGF-β [29, 31, 34]. We initiated an EMT response (Supplementary Figure 6a) and observed changed morphology as well as loss of WT1 and ZO1 indicating loss of epicardial identity and demonstrating the functionality to transition into EPDCs (Figure 2i). The identity of induced CFs (iCFs) and induced SMCs (iSMCs) was validated by expression of POSTN and αSMA respectively (Figure 2i). We also sequenced the whole transcriptome of iCFs and iSMCs, verifying distinct cellular identities by PCA (Supplementary Figure 6b), as well as enrichment of respective gene signatures (Figure 2j). We then analyzed *CDH18* expression in epicardial derivatives from both PE-like d12 and fetal-like d24 EPI cells. *CDH18* was lost in iCF and iSMC (Figure 2k-l and Supplementary Figure 6c-f), demonstrating that reduced levels of *CDH18* correlated to a loss of EPI identity. Loss of CDH18 upon EMT was also confirmed in murine epicardial MEC1 cell line (Supplementary Figure 6d).

Taken together, our results demonstrate that CDH18 is a specific active epicardial biomarker and suggest a causal role in specification and maintenance of epicardial identity.

Loss of *CDH18* triggers cell-fate specific EMT towards smooth muscle cells

To explore the biological relevance of *CDH18*, we next silenced *CDH18* gene expression in d24 EPI cells (d24•si18) (Figure 3a). The downregulation of *CDH18* (Figure 3b-d) led to visible morphological changes with a fraction of cells becoming elongated and losing the cobblestone-like morphology (Figure 3d, yellow arrowheads) indicating a switch to mesenchymal cells [42]. Cells that retained epicardial morphology were in close contact, suggesting that cell-cell interactions might play a role in maintaining EPI identity. Similar results were obtained using a second siRNA (Supplementary Figure 7a-c). *CDH18*-silenced cells showed reduced growth (Figure 3e) suggesting that *CDH18* downregulation in fetal-stage epicardium may confer either a proliferative disadvantage impairing epicardium homeostasis and expansion or defines the triggering signal for EMT initiation. We observed gain of SNAI1 expression (Figure 3f) upon *CDH18* downregulation, thus indicating the initiation of EMT. Confirming this functional onset, we observed a strong downregulation of *CDH1* (E-cadherin). However, upregulation of *CDH2* (N-cadherin) (Figure 3g) was only modest.

A previous report showed that epicardial cells are more prone to undergo EMT during the early stages of development [43, 44]. We therefore questioned, if fetal-like d24 EPI cells were more resistant to initiate EMT than d12 EPI cells, a time-point that portrays a more PE-like state. Accordingly, we silenced *CDH18* in d12 EPI cells (d12•si18) finding similar morphofunctional changes as in d24 EPI cells (Figure 3h-j and Supplementary Figure 7d-f). Loss of CDH18 was accompanied by gain of SNAI1 (Figure 3h) and d12•si18 cells showed changed morphology, reduced growth as well as decreased levels of Ki67 (Supplementary Figure 7f-g and Figure 3l), thus indicating the onset of EMT. Notably, the switch from *CDH1* to *CDH2* was much stronger in d12 silenced cells, implying the acquisition of mesenchymal identity (Figure 3j). Furthermore, *CDH18*-silenced cells showed enhanced migration (Figure 3k), endorsing that the downregulation of *CDH18* leads to a loss of epicardial identity towards the EPDC-like state. To exclude that our observations were biased due to an early loss of cells we also confirmed that cells displayed reduced proliferation marker expression Ki67, upregulation of SNAI1 and loss

of ZO1 3-4 days after silencing (Supplementary Figure 7h-o), further strengthening, that cells were undergoing EMT upon CDH18 downregulation.

Several pathways are reported to be involved in the regulation of EMT [45-54], with Wnt pathway regulation by Wt1 being linked to epicardial development and cell differentiation [6], as well as cardiac regeneration[55]. Cadherins are known to exert their functions through phosphorylation-mediated protein stabilization of β-catenin in the Wnt signaling pathway [56, 57]. Moreover, a previous report has shown the direct interaction of Cdh18 with β-catenin [58]. We therefore hypothesized that CDH18 might manage its impact on epicardial EMT via regulation of β-catenin. Indeed, we observed that loss of CDH18 lead to increased levels of β-catenin with decreased phosphorylated (p)-β-catenin as well as increase in LEF1 (Figure 3l and Supplementary Figure 7m-n), indicating the activation of the Wnt pathway.

Interestingly, we found reduced levels of TCF21 upon *CDH18*-silencing (Figure 3l). *TCF21* acts as an epicardial marker playing pivotal roles during EMT and EPDC-fate regulation between CF and SMC [59-61]. EPI cells showed increased *TCF21* expression at the mRNA and protein levels (Supplementary Figure 8a-b). Reduced levels of TCF21 implies differentiation towards a SMC rather than a CF fate [7, 60]. To confirm this hypothesis, we compared the expression levels of SMC genes in *CDH18*-silenced EPI cells and iSMCs. We found that *CDH18*-silenced cells recapitulated the iSMC expression levels of *ACTA2* and *CNN1* specially in d12 silenced cells and to a lesser degree also in d24 silenced cells (Figure 3m and Supplementary Figure 8c-e). Canonical TGFβ-pathway activation seemed to play a noteworthier role for EMT onset in fetal-like d24 compared to PE-like d12 cells, as TGFβ inhibitor withdrawal does enhance the expression levels of *ACTA2* in fetal-like d24 cells (Supplementary Figure 8e). To assess the role of non-canonical activation, we tested the impact of ROCK, inhibitor impairing RhoA-mediated pathway, on CDH18 downregulation in d12 cells. While no significant change could be observed in SNAI1 expression, *ACTA2* expression was reduced by ROCK inhibition, albeit only when TGFβ signaling was not blocked (Supplementary Figure 8f). The acquisition of an SMC-like identity in *CDH18*-silenced cells was further verified by the loss of ZO1 and the expression of α-SMA (Figure 3n).

Next, we aimed to investigate the transcriptional contribution of *CDH18*-downregulation to the SMC phenotype and the enhanced potential to derive SMC-like cells from d12 PE-like cells compared to d24 fetal-like cells. We therefore performed RNA-Seq and showed a transcriptome distribution of up to 99.4% combined variance by PCA (Figure 4a). PE-like *CDH18*-silenced cells were allocated within the same arm as iSMCs, mapped closer to iSMC and mapped more DEGs (Figure 4a-b and Supplementary Figure 9a-b). The downregulation of *CDH18* suppressed epicardial identity both at the fetal-like stage and PE-like stage and activated the SMC gene program, while CF-related genes remained unaffected (Figure 4c-d and Supplementary Figure 9c). Specifically, in d12 PE-like stage cells silencing of *CDH18* influenced gene categories supporting SMC acquisition (Figure 4c) and showed a greater expression of important markers of EMT activation (Figure 4f). The altered expression of important cell cycle checkpoint regulators confirmed reduced proliferation upon *CDH18* downregulation (Figure 4g). Finally, we analyzed gene signatures to identify activated signaling pathways, finding that TGF-β and Wnt pathway, which are known to contribute to the SMC phenotype, were affected and activated upon *CDH18* downregulation (Figure 4h-i).

Altogether, we confirmed that *CDH18* is an important regulator of the SMC phenotype. *CDH18* downregulation led to a loss of epicardial cell identity under the retained inhibition of TGF-β, a situation that normally sustains epicardial hallmarks. The role of *CDH18* is essential in epicardial fate and plasticity determination during human development, especially if the loss of *CDH18* occurs at an early stage of epicardial specification.

CDH18 is unable to block TGF-β-driven EMT towards SMC differentiation

To investigate the potential of *CDH18* expression to regulate epicardial maintenance and SMC differentiation, we evaluated the capacity of *CDH18* to inhibit the initiation of EMT towards SMC differentiation. We ectopically overexpressed human *CDH18* cDNA (Supplementary Figure 10a) in d12 EPI cells, which we assessed via mCherry expression, and subsequently induced EMT towards iSMC formation (Figure 5a). Unfortunately, EPI cells were difficult to transfect, consistent with a previous report on mouse epicardial-like cells [34, 48]. Optimization of the transfection efficiency (Supplementary Table 1) led to ~25% of cells expressing mCherry at d3 post transfection (Figure 5b-c and Supplementary

Figure 10b). To obtain a pure *CDH18*-overexpressing population, we then sorted mCherry-expressing cells (mCherry+) (Supplementary Figure 10c). The gain of *CDH18* expression was confirmed in unsorted and sorted settings (Figure 5d), and CDH18 protein gain was confirmed in mCherry+ cells (Figure 5e).

Next, we analyzed the effect of *CDH18* overexpression during iSMC induction. We did not observe morphological differences between conditions (Figure 5f). Nevertheless, *CDH18*-overexpressing cells showed fewer iSMCs (Figure 5f), hinting at a potential role of *CDH18* in maintenance of the active epicardium. All populations showed less *CDH18* expression upon treatment with TGF-β and bFGF (Figure 5g), but transfected cells retained *CDH18* expression even after undergoing EMT. In agreement with the morphological SMC phenotype (Figure 5f), all populations showed increased *ACTA2* expression upon iSMC induction (Figure 5h). Notably, *ACTA2* levels were significantly reduced in cells still expressing *CDH18*. RNA-Seq analysis revealed the reduced expression of several SMC markers in CDH18-overexpressing SMCs (Figure 5i), highlighting an important role of CDH18 preventing the fully SMC identity acquisition. During development, not only differentiation of epicardial cells into SMC, but also their migration is important for successful coronary artery formation [62-64]. To investigate the functional properties of *CDH18*-overexpressing cells, we next tested their invasion ability. We compared EPI cells to cells undergoing spontaneous EMT in absence of TGFβ inhibitor and CDH18-overexpressing SMCs (Figure 5j). In all conditions CDH18-overexpressing cells showed reduced invasion capacity. We therefore concluded, that although ectopic *CDH18* overexpression cannot fully block the TGF-β-driven differentiation to SMC, it partially impairs the acquisition of SMC identity and their functional properties.

CDH18* expression is under the control of *GATA4

Finally, to elucidate the regulation of *CDH18* in epicardiogenesis, we identified 23 transcription factors out of 522 genes that are in correlation with *CDH18* and enriched in late-stage active epicardium (Figure 6a-b). Among these transcription factor encoding genes, only GATA4 showed a high relative score to bind the *CDH18* promoter (Figure 6c and Supplementary Figure 11a). During EPI induction *GATA4* is expressed in associative

correlation to *CDH18* (Supplementary Figure 11b-c and Figure 6d). *GATA4* is a well-characterized regulator at early cardiogenesis playing a pivotal role in PE formation. *GATA4*-null mice embryos fail to form the epicardium due to impaired PE development, thus being an essential gene in epicardiogenesis. We therefore silenced *GATA4* using two siRNAs (siGata4#1 and siGata4#2) at different time points during epicardial differentiation: at d5 of epicardial induction marking the beginning of cell development towards PE-like stage and at d12 marking the specification towards fetal-like epicardium (Supplementary Figure 11d). *GATA4*-silenced cells showed reduced cell survival (Figure 6e, upper panel), but surviving clones did not alter *GATA4* levels (Supplementary Figure 11e) and were able to reconstitute after 7 days (Figure 6e, lower panel) showing no significant reduction of either *GATA4* or *CDH18* expression (Figure 6e-f). Thus, implying that upon efficient silencing of *GATA4*, cells were not able to survive. We therefore concluded that *GATA4* is necessary for cells at d5 to differentiate towards the PE-like state. Next, we downregulated *GATA4* in d12 EPI cells and observed some morphological changes after siRNA administration over time (Figure 6g, yellow arrowheads). The downregulation of *GATA4* was accompanied by *CDH18* downregulation in a similar fashion on both mRNA (Figure 6h and Supplementary Figure 11f) and protein level (Figure 6i). Thus, these results promote *GATA4* as a putative regulator of *CDH18* expression, highlighting their relevance for formation and specification of active epicardium.

DISCUSSION

The epicardium is essential for cardiogenesis and its re-activation upon injury during adulthood is indispensable for cardiac regeneration. Exploiting epicardial targeting to model cell therapy-based approaches for cardiac repair and regeneration requires a detailed knowledge of the mechanisms that regulate the active epicardium. Here, we recapitulated the human epicardiogenesis using hiPSCs and defined a surfaceome of human active epicardium that is later inactivated in the quiescent (adult) epicardium. We define *CDH18* as an epicardial biomarker that is exclusively expressed in epicardial cells compared to their derivatives and other cardiac cell types. The epicardium specificity of *CDH18* expression can be used as a specific, rather than associated, active epicardial biomarker to both define biological identity and modulate EMT-specific processes towards SMC. Previous identification of epicardial cells was based on the expression of several transcription factors such as *WT1*, *TBX18* and *TCF21*. However, their expressions are not restrictive to the epicardium. Our findings provide a molecular alternative for the identification of epicardial cells by tracing *CDH18* expression, a biomarker of the active fetal epicardium.

Cadherin 18 (CDH18), formerly named cadherin 14, is a type II classical cadherin predominantly expressed in the central nervous system, contributing significantly to axonal development and maintenance [38-40]. This study succeeded in documenting murine CDH18 in fetal heart explant culture, known to be derived from the epicardium. Given the thin-shaped nature of the epicardium, its density represents a notable minority in the context of the human heart. We did not detect protein expression in whole trypsinised whole-heart lysates, as mostly cardiomyocytes were isolated. In addition, our study suggests that *CDH18* expression shapes the fetal active epicardium transcriptome, but is downregulated in quiescent adult tissue [4, 65], thus explaining why *CDH18* remained undetected in the heart [40].

Investigating the expression of CDH18 in human embryonic epicardial cells *in vivo* is technically difficult due to lack of technical approaches to trace epicardial development as well as limited availability of human fetal cells. The use of hiPSC overcomes this issue by enabling recapitulation of epicardiogenesis *in vitro*. Whereas our study limits our main

conclusions to *in vitro* differentiated epicardial cells and their derivatives, we believe that our key discoveries are physiologically relevant, since RNA-Seq based meta-analysis shows that *CDH18* is expressed in human heart during the third month of gestation, a time point of active development of the cardiovascular system in the human embryo, being in line with the hiPSC-based model shown in this study. Moreover, we documented murine embryonic CDH18 expression in epicardial explant cultures from E14.

Recent reports demonstrate an essential role for *WT1* in epicardial cell specification and maturation from the PE, suggesting that junction remodeling is crucial for this transition [66, 67]. We showed that *CDH18* is expressed in correlation to *WT1* during epicardial development, leading us to hypothesize that *CDH18* might play a critical role for the specification and maintenance of epicardial cell identity, similar to *WT1*.

During human heart formation as well as during cardiac repair epicardial cells also contribute to coronary vessel formation by providing necessary vascular SMC and pericytes, which invade the myocardium. Notably, we provide compelling evidence to indicate that *CDH18* is critical for the modulation and establishment of epicardial-derived SMCs. We proved that *CDH18* downregulation modulates the expression of EMT markers and impacts epicardial identity. Recent studies characterized a *CDH18* tumor-suppressor role in glioma carcinogenesis and progression, demonstrating an active role in invasion and cell migration [38], important processes that also relate to cardiac regeneration. The ectopic overexpression of *CDH18* was reported in relation to decreased migration capacity in accordance with our study. Most importantly, our study gained mechanistic insights into the biological regulation during the initiation of EMT in epicardial cells. The loss of *CDH18* decreased proliferation, *CDH1* expression and β-catenin. Interaction with and regulation of stabilization of β-catenin via cadherins is critical for cellular organization, polarity and development [56, 57]. Indeed, a previous study showed that Cdh14 interacts with and stabilizes β-catenin, similar to Cdh1 [58]. Another study reported, that type II Cdh14 (Cdh18) along with type I E-cadherin (Cdh1) and N-cadherin (Cdh2) can bind to G12 family proteins [68], which are known to regulate β-catenin translocation from the cell surface, a function associated with Rho-dependent cytoskeletal rearrangement. In our study, we demonstrated that the loss of CDH18 increased β-catenin levels, indicating Wnt

activation and the promotion of EMT. The activation of Wnt signaling via β-catenin has long been deemed important for epicardial EMT and SMC differentiation which known to be regulated by Wt1 [6, 7, 29, 53, 69, 70]. Although controversial [52], our study supports the necessity of β-catenin for SMC differentiation *in vitro* [70].

TCF21 is another key regulator of epicardial plasticity and EMT, promoting CF over SMC fate [60]. It is possible that rather than the activation of specific signaling pathways, the expression of TCF21 is of far greater importance for cell-fate decision. Thus, investigating Wnt and TGF-β signaling pathways and their influence on *TCF21* could shed more light on this area, which will also allow to understand cell-fate decisions during cardiac regeneration, in particular those physiological stimuli that presumably force cells to assume a CF rather than pericyte phenotype. In addition, *TCF21* is known to be induced by retinoic acid (RA), thereby delaying SMC differentiation [60, 71, 72]. We showed that the expression of *ALDH1A2* is not upregulated until d24 and low in d12 EPI cells. Thus, our observation of d24-silenced cells expressing lower levels of the SMC marker *ACTA2* could be linked to the higher presence of RA and *TCF21* in fetal-like cells compared to PE-like cells. During cardiac repair, expression of *ALDH1A2* is re-activated, which might explain the preferred CF fate of epicardial cells that undergo EMT upon re-activation. Here, we showed loss of TCF21 upon loss of CDH18, suggesting a role for β-catenin-mediated Wnt activation in SMC differentiation. Furthermore, this observation occurred under the inhibition of the TGF-β co-receptor ALK5, which is known to impair EMT [73]. Our findings provide new insights of the regulation of the EMT process as a crucial step mediating epicardial-driven regenerative responses.

The exact mechanisms governing epicardial EMT and subsequent cell-fate decision of EPDCs in active epicardium are not well understood. Most experiments have used chick, avian or mouse models, which can differ considerably from human. We observed the activation of downstream TGF-β signal targets, confirmed by RNA-Seq, upon *CDH18* silencing albeit treatment with SB431542. Our study endorses the link between TGF-β signaling and SMC phenotype [29, 31, 34, 70], as we observed SMC differentiation and TGF-β activation upon lower *CDH18* expression. Although *CDH18* overexpression could not completely block TGF-β-driven SMC differentiation, we found a partial prevention in the

acquisition of SMC identity, indicated by lower levels of *ACTA2*. Altogether, our findings indicate a causal role of *CDH18* in TGF-β pathway during the acquisition of SMC identity.

CDH18 is a cell surface protein linked to G12 family proteins [68], and RhoA pathway-mediated non-canonical TGF-β pathway, which has been linked to EMT and cell invasion [45, 48-50, 74, 75], might be activated upon the silencing. Interestingly, one study showed that inhibition of the RhoA pathway does not influence canonical TGF-β activation but still impairs SMC formation [76]. In our study, however, for those experiments that kept ALK5 inhibition conditions, ROCK inhibitor did not alter SMC marker expression upon CDH18 silencing. Only when ALK5 inhibitor was absent, did inhibition of ROCK lead to a decrease in ACTA2.

Recently, a new study linked a TGFβ-independent causal role of the extracellular matrix (ECM) protein agrin to epicardial EMT mediated by dystroglycan [17]. This report also showed that their findings occur via WNT signaling activation, a phenotype that could have common denominators with our study. Future studies are needed to shed more light into the different behavior of cells during human epicardial development. Such studies will also help deepen our understanding of epicardium re-activation upon cardiac injury and advance the field of cardiac regenerative medicine.

Finally, we demonstrated the correlative relationship between CDH18 and *GATA4* expression, proposing *GATA4* as a putative regulator of *CDH18*. This effect likely occurs by static binding to the *CDH18* promoter near the transcriptional starting site, reinforcing *GATA4* as an important activator of the embryonic epicardium program.

CDH18 is a highly conserved protein in higher mammals and species that evolutionary developed a double closed circulatory system, maintaining an amino acid alignment of over 95% identity and 100% query sequence coverage relative to humans. The conserved sequence suggests that CDH18 has remained relatively unchanged far back up the phylogenetic tree in species developing a higher compartmentalized system to create a physical separation of oxygenated and deoxygenated blood (Supplementary Figure 12). A higher demand of SMC might explain CDH18 conservation in development (Supplementary Figure 13). Altogether, these findings indicate a specific role for CDH18

in epicardial regeneration and development, both processes that are under the control of evolutionary conserved pathways

In conclusion, our work defines a biological function of *CDH18* in the epicardial context, enabling roads for the manipulation and therapeutic gene modulation of the active epicardium for cardiac repair and regeneration.

METHODS

Cell lines and Culture Conditions

The hiPSC lines 201B7 and 409B2 (retroviral reprogramming by Yamanaka factors) (REF16) as well as a MYH6-eGFP reporter cell line (MYH6-EIP4) (REF31) were cultured in ReproCell ES media containing 4 ng/ml bFGF on irradiated MEF feeder cells. For removal of the feeder layer, the cells were treated with CTK. Feeder-free 201B7 were cultured in complete StemFit® AK02N media on iMatrix-511 (Matrixome) coated dishes. All cell lines used were female. Mycoplasma testing was performed on a regular basis to exclude contamination.

Epicardial induction

For epicardial differentiation, single cell suspension of hiPSC was generated using Accutase and subsequently cells were plated onto low-attachment HEMA-coated plates (6000-8000/96-well) to form embryoid bodies (EBs). Differentiation media was composed of complete StemPro®-34 media supplemented with 50 µg/ml ascorbic acid, 2 mM L-glutamine, 0.4 µM monothioglycerol and 150 mg/ml transferrin. To initiate differentiation, 0.5% Matrigel, 10 µM Y-27632 and 2 ng/ml human recombinant (hr)BMP4 were added to the differentiation media. After 24 hours (h) EBs were cultured in differentiation media with a final concentration of 10 ng/ml hrBMP4, 2 ng/ml Activin A and 5 ng/ml hrbFGF. After 84 h, EBs were collected, dissociated using Accutase, and plated onto 0.1% gelatin-coated dishes (0.3 x 10^5 cells/cm^2) in differentiation media containing 3 mM CHIR99021, 30 ng/ml hrBMP4, 5 ng/ml hrVEGF and 10 µM SB431542. From d7 onwards, induced hiPSC-derived epicardial-like (EPI) cells were maintained in maintenance media (DMEM containing 10% FBS and 10 µM SB431542). For cell passaging, EPI cells were detached by Accutase treatment for 5 min and replated as described above.

Cell transfection

For the silencing experiments, Silencer® Select siRNAs (ThermoFisher) were diluted to a 10 µmol stock solution: siCdh18#1 (s2816), siCdh18#2 (s2817), siGata4#1 (s535120) and siGata4#2 (s535121). To silence cells, 10 µl siRNA stock was diluted in 500 µl Opti-MEM, and 10 µl RNAiMax was added (silencing solution) followed by 10 min incubation

at room temperature. The solution was added dropwise into one well of a 6-well plate containing 2 ml maintenance media and 0.2-0.3 x 10^5 cells seeded a day prior. The media was exchanged 24 h later, and the cells were cultured as usual thereafter. For the immunocytochemistry experiments, 260 µl silencing solution was added dropwise into one well of a 12-well plate containing 1 ml maintenance media and 0.05 x 10^5 cells seeded a day prior to silencing.

For *CDH18* cDNA overexpression experiments, the cells were seeded to be 60-70% confluent at least one day prior to the transfection. For optimization of transfection protocol, transfection reagents and ratios as well as the plasmid amount were used as indicated in Supplementary Table 1. Unless otherwise stated, 6 µg plasmid per one well of a 6-well plate or 17 µg plasmid per 10 cm dish were transfected using FuGENE®6 at an agent-to-DNA ratio of 2:1. Amounts of reagents were calculated using FuGENE®HD Protocol Database web tool. Cell sorting was performed by FACS via assessment of mCherry expression (Texas-Red positive cells).

Induction of EMT

For the induction of EMT, EPI cells were passaged one day prior, at a density of 0.1-0.2 x10^5 per well of a 6-well plate. For differentiation towards CF, the cells were treated with 10 ng/ml bFGF in 10% FBS DMEM for at least 8 days. For differentiation towards SMC cells were treated with 5 ng/ml TGF-β for 4 days followed by 10 ng/ml bFGF for another 4 days in 10% FBS DMEM.

Isolation of mouse fetal hearts and whole-heart lysate

Embryos at E14 were collected into pre-warmed PBS and any extraembryonic tissue was removed using tweezers. Embryos were decapitated, the chest cavity was opened by ripping the anterior side apart and fetal hearts were isolated mechanically into a separate dish with pre-warmed PBS. Whole heart protein lysate was prepared by firstly cutting hearts into small pieces and treatment with trypsin for 20min at 37ºC. Cell suspension was re-suspended, treated for additional 20min at 37ºC and supernatant was collected after centrifugation at 300g for 5min.

Ex vivo explant assay

Collected hearts at E14 were cut into 4-8 pieces and placed onto 0.1% gelatin-coated dished in DMEM (low glucose) supplemented with 15% FBS. Outgrowth cultures formed as early as 24h post placing. After 72h heart pieces were manually removed with tweezers. Explant cells were passage by trypsinization the following day and cultured in 10% FBS-DMEM (low glucose) supplemented with 10 µM SB431542. Cells were collected 1-3 days after passage. EMT was induced as described above in 10% FBS-DMEM (low glucose).

Quantitative RT-PCR

For RNA extraction, live cells were collected as du- or triplicate in QIAzol lysis reagent, and total RNA isolation was performed using the RNAeasy micro kit (Qiagen) according to the manufacturer's manual. The generation of cDNA was performed by using the ReverTra Ace system (Toyobo BIOTECH) according to the manufacturer's manual. QRT-PCR was performed in du- or triplicate either using TaqMan gene expression assays (*WT1* Hs01103750_g1; *TBX18* Hs01385457_m1; *ALDH1A2* Hs00108254_m1; *TCF21* Hs00162646_m1) in TaqMan master mix solution or SYBR green (ThermoFisher) with primers against identified candidates (Supplementary Table 2) in SYBR green master mix solution according to the manufacturers' respective manuals. Data acquisition was carried out by StepOne Plus (AppliedBiosystems). Analysis was performed using Microsoft Excel and GraphPad Prism. Values without readout were not included. The distribution of values was verified by a box plot depiction to determine the appropriate statistical analysis. For direct comparison of dataset normally distributed data was analyzed by students t-test, as indicated in figure legends, otherwise the Mann-Whitney test was used. Comparisons of more than two datasets were carried out via ANOVA, according to experimental conditions, as indicated in the figure legends. All error bars represent standard error of the mean (SEM). For co-expression analysis, qRT-PCR data was used to generate a regression line by GraphPad Prism v7 and higher.

Immunocytochemistry

Cells were fixed by 4% PFA treatment for 15 min and stored in PBS at 4ºC. Blocking was performed for 30-45 min in blocking buffer: 1% BSA and 0.5% Triton X for nuclear staining

or 0.1% Tween 20 for surface or intracellular staining and 0.1M glycine in PBS. Following three PBS washes, primary antibody was added in blocking buffer without glycine and incubated overnight at 4ºC. The primary antibodies used are as follows: Anti-WT1 1:200 (Abcam; ab89901), Anti-ZO1 1:100-300 (Invitrogen; ZO1-1A12), Anti-POSTN 1:200 (ThermoFisher; PA5-98301), Anti-α-SMA 1:200 (Abcam; ab7817) and Anti-Ki67 1:200 (BioLegend; 350502). The next day, the cells were washed thrice with PBS, secondary antibody (Invitrogen, 1:1.000-2.000) was added in 1% BSA-PBS and incubated for 2 h at room temperature. The secondary antibodies were used are as follows: goat-anti-mouse-Alexa488 (A11001), goat-anti-rabbit-Alexa546 (A11010), goat-anti-mouse-Alexa546 (A11030), goat-anti-mouse-Alexa594 (A11032), goat-anti-rabbit-Alexa647 (A21245), goat-anti-mouse-Alexa647 (A21236). Following three washes with PBS, Hoechst or DAPI (5 ng/ml, 1:10.000) was added for nuclear counterstaining.

Flow cytometry analysis/FACS

Cell were dissociated into single cell suspension by Accutase treatment, washed twice and fixed using 4% PFA for 15 min. For nuclear staining, the cells were permeabilized by 0.1% Triton X solution. Conjugated antibodies were diluted 1:50 in FACS buffer (5% FBS-PBS) and incubated at room temperature for 30-45 min. The conjugated antibodies used are as follows: WT1-Alexa488 (Abcam; ab202635), rb-IgG-Alexa-488 (Abcam; ab199091), CDH18-FITC (Biorbyt Ltd; orb7854), CD22-APC (BD; 562860) CD31-APC (BioLegend; 303116) and CD144-FITC (BD; 560874).

For sorting, a single cell suspension was generated as described above, and counterstaining with 1:10.000 DAPI (5 ng/ml) was performed for death cell exclusion. Sorting gates were set as described.

Analysis was performed using BD FACSDiva v6 or v8 and FlowJo v10. Cell population was identified by FSC/SSC gating and doublets discrimination was performed. Negative gates were established using unstained samples or isotype controls and negative control samples. Positive gates were set to contain no negative signal.

Immunoblotting

Cells were detached using Accutase and lysed in Mammalian Protein Extraction Reagent (M-PER) (Thermo Scientific; 78501) buffer. The amount of protein was determined by the

Bradford assay using BSA as the standard. The primary antibodies (dilution 1:1000) used are as follows: Anti-CDH18 antibody (Proteintech 13091-1-AP), Anti-GATA4 (CST; 369665S (D3A3M)), Anti-SNAI1 (Abcam; ab63371), Anti-α-SMA (Abcam; ab11952), Anti-β-actin (Sigma; A5441), Anti-WT1 (Abcam; ab89901), Anti-CD22 (Abcam; ab207727), Anti-TCF21 (Abcam; ab32981), Anti-β-catenin (CST; 8814), Anti-phosporylated-β-catenin (S33/S37/T41) (CST; 9561). The secondary antibodies (dilution 1:5000) used were as follows: goat anti-rabbit-horseradish peroxidase (HRP) (Abcam; ab97051), rabbit anti-mouse-HRP (Abcam; ab97046).

Proliferation assay

A time course curve of parental (scr) and siRNA-expressing cells was generated by seeding 4.5 x 10^3 cells into 6-cm bottom-well diameter dishes. After 24 h, fresh medium was replaced and cells were fixed to be referred as a standard for relative growth (day 0). Relative growth was assessed every 48 h (2 days), fixing in 2% PFA and stained with 1% crystal violet (Sigma; C6158-50G). After extensive cell washing, crystal violet was solubilized in 20% acetic acid (Sigma) and quantified absorbance at 595 nm as a relative assessment of cell number (PerkinElmer; EnVision 2104 Multilabel Reader). Relative values in Figure 4 represents cell growth of daughter the indicated medium. Percentage zero (0%) refers to initial growth at day 0.

Invasion assay

Cell were silenced as described above and collected 4 days later. 2.5 x 10^4 cells were seeded onto a Corning® Biocoat® Matrigel® Invasion chamber and incubated for 24 h or 48 h. The removal of non-invasive cells was carried out as stated in the Corning® Biocoat® Matrigel® Invasion manual, and the cells were fixed for 2 min in methanol followed by staining using crystal violet overnight and finally washed with distilled water. Pictures were taken using BZ-X710 (Keyence) and cell counting was performed with ImageJ. Cell counting was performed blinded using ImageJ v1.52. Images were converted to 8-bit greyscale format, and the same threshold was set for all images to highlight cell structures. Potential cell clusters were separated by the watershed function, and only structures 0.01-0.1 $pixel^2$ in size were counted. Graphs were generated using GraphPad Prism v8.

Bioinformatics

Retrospective analysis of *CDH18* gene expression was done using GSE84085 (GEO) for epicardium development and GSE7307 for cardiovascular derived tissues (subset of aorta, coronary artery, heart, heart atrium and heart ventricle) [GEO and R2; genomic analysis and visualization platform (http://r2.amc.nl/)].

Promoter sequences were identified by *Ensembl* and then screened for transcription factor binding sites with PROMO-ALGGEN (based on TRANSFAC v8.3) and JASPAR 2016.

Image acquisition, processing and analysis

Microscopy images were taken by BZ-X710 and processed by BZ-X Analyzer (Keyence); pseudo-coloring was used as indicated in figure legends. For phase contrast and fluorescence pictures a representative section was chosen, cropped and magnified. Western blot data was recorded by LAS4000 (Cytiva). General image analysis was performed using Microsoft power point as well as ImageJ v1.52.

RNA-sequencing

Data normalization was carried out using NOISeq. The final processed data and raw fastq files generated de novo in this study were submitted to Gene Expression Omnibus (GEO) under the accession code GSE165450. The raw data were analyzed by using RStudio for further analysis on gene expression. Gene expression data for reading, exploring and pre-processing were conducted using the Bioconductor package *NOISeq* pipeline to perform data and differential expression analysis for RNA-Seq. A hierarchical derived cluster dendrogram was generated by using hclust, *stats* package, and *agnes* in the *cluster* package. Distances were assessed by using Manhattan city-block distance algorithm. K-means were calculated with the kmeans function. Distance and correlation matrices were computed and plotted by using *get_dist*, *fviz_dist* included in the *factoextra* package. The *fviz_cluster* function was used to compute cluster scatter plots. Heatmaps were depicted to cluster the expression data for DEGs using R script. Statistical analysis and visualization of the functional profiles of genes as well as gene clusters for GO terms were conducted using the *DOSE* and *clusterProfiler*. Ingenuity pathway analysis (IPA)

was used to develop an upstream pathway analysis as well as pathway activity patterns. Chord diagrams were generated by using GOplot.

Material availability

The CDH18 overexpression plasmid used in this study is available from VectorBuilder [VB200615-1011cyh]. Other materials are available from the corresponding author upon reasonable request, but we may require payment and/or a Materials Transfer Agreement.

Animal experiments

All experiments involving animals were approved by the Kyoto University Animal Experimentation Committee and carried out in accordance to the Guidelines for Animal Experiments of Kyoto University and Guide to the Care and Use of Laboratory Animals by the Institute of Animal Resources.

DATA AVAILIBILITY STATEMENT

Data availability

All data supporting this study are available within this publication and its supplementary information or can be provided upon request. The RNA-Seq dataset generated in this study is deposited at Gene Expression Omnibus (GEO) with the accession code GSE165450.

ACKOWLEDGMENTS

We would like to thank Professor Shinya Yamanaka and all members of the Yoshida laboratory for their constructive feedback on this study. J.J. thanks the Japanese Government (MEXT) scholarship for its financial support. This work was supported by a grant from the Leducq Foundation (18CVD05) and JSPS KAKENHI Grants (20K17078 (A.L-C), 21H02912 (Y.Y.), and 17H04176 (Y. Y.)). Funding is also provided by the Research Center Network for Realization of Regenerative Medicine, Japan Agency of Medical Research and Development (AMED) (JP19bm0104001, JP19bm0804008, JP20bm0204003, and JP20bm0804022) (Y.Y.), the Research on Regulatory Science of Pharmaceuticals and Medical Devices, AMED (JP19mk0104117) (Y.Y.), the Research Project for Practical Applications of Regenerative Medicine, AMED (JP19bk0104095) (Y.Y.), the iPS Cell Research Fund (A.L-C and Y.Y.) and the SECOM Science and Technology Foundation (Y.Y.). We would like to express our heartfelt gratitude to Peter Karagiannis for proofreading and advice in manuscript writing, Kazuhisa Chonabayashi for providing control cells, Yoko Uematsu, Kaoru Shimizu and Mikako Marx Mori for their administrative support.

DECLARATION OF INTERESTS

JJ., T.Y, Y.K., E.M.V-S., M.N. and A.L-C declare no competing interest. Y.Y. is a scientific advisor of Orizuru Therapeutics.

AUTHOR CONTRIBUTIONS

J.J., A.L-C. and Y.Y. conceived the study and designed the experiments. J.J. and A.L-C. performed the experiments analyzed and interpreted the data, Y.K. assisted with the immunocytochemistry experiments and analysis, T.Y. validated the qRT-PCR experiments, E.M.V-S. generated chord diagrams and performed a retrospective analysis of the protein sequence. M.N. assisted with the RNA-Seq experiments. Y.Y. and A.L-C provided funding and supervision. J.J., A.L-C. and Y.Y. wrote the manuscript. All authors discussed the results.

REFERENCES

1. Bargehr, J. *et al.* Epicardial cells derived from human embryonic stem cells augment cardiomyocyte-driven heart regeneration. *Nat Biotechnol* **37**, 895-906 (2019).
2. Pérez-Pomares, J.M. & de la Pompa, J.L. Signaling during epicardium and coronary vessel development. *Circulation Research* **109**, 1429-1442 (2011).
3. van Wijk, B. & van den Hoff, M. Epicardium and myocardium originate from a common cardiogenic precursor pool. *Trends Cardiovasc Med* **20**, 1-7 (2010).
4. Zhou, B. *et al.* Adult mouse epicardium modulates myocardial injury by secreting paracrine factors. *The Journal of Clinical Investigation* **121**, 1894-1904 (2011).
5. Gittenberger-de Groot, A.C., Vrancken Peeters, M.P., Mentink, M.M., Gourdie, R.G. & Poelmann, R.E. Epicardium-derived cells contribute a novel population to the myocardial wall and the atrioventricular cushions. *Circ Res* **82**, 1043-1052 (1998).
6. von Gise, A. *et al.* WT1 regulates epicardial epithelial to mesenchymal transition through β-catenin and retinoic acid signaling pathways. *Dev. Biol.* **356**, 421-431 (2011).
7. Braitsch, C.M. & Yutzey, K.E. Transcriptional Control of Cell Lineage Development in Epicardium-Derived Cells. *Journal of Developmental Biology* **1**, 92-111 (2013).
8. Katz, T.C. *et al.* Distinct compartments of the proepicardial organ give rise to coronary vascular endothelial cells. *Dev. Cell* **22**, 639-650 (2012).
9. Zhou, B. *et al.* Epicardial progenitors contribute to the cardiomyocyte lineage in the developing heart. *Nature* **454**, 109-113 (2008).
10. Krainock, M. *et al.* Epicardial Epithelial-to-Mesenchymal Transition in Heart Development and Disease. *J Clin Med* **5** (2016).
11. Smart, N., Dube, K.N. & Riley, P.R. Coronary vessel development and insight towards neovascular therapy. *Int J Exp Pathol* **90**, 262-283 (2009).
12. van Wijk, B., Gunst, Q.D., Moorman, A.F. & van den Hoff, M.J. Cardiac regeneration from activated epicardium. *PLoS One* **7**, e44692 (2012).
13. Rao, K.S. & Spees, J.L. Harnessing Epicardial Progenitor Cells and Their Derivatives for Rescue and Repair of Cardiac Tissue After Myocardial Infarction. *Curr Mol Biol Rep* **3**, 149-158 (2017).
14. Cao, Y. & Cao, J. Covering and Re-Covering the Heart: Development and Regeneration of the Epicardium. *J Cardiovasc Dev Dis* **6** (2018).
15. Ramjee, V. *et al.* Epicardial YAP/TAZ orchestrate an immunosuppressive response following myocardial infarction. *J Clin Invest* **127**, 899-911 (2017).
16. Wei, K. *et al.* Epicardial FSTL1 reconstitution regenerates the adult mammalian heart. *Nature* **525**, 479-485 (2015).
17. Sun, X. *et al.* The extracellular matrix protein agrin is essential for epicardial epithelial-to-mesenchymal transition during heart development. *Development* **148** (2021).
18. Walma, D.A.C. & Yamada, K.M. The extracellular matrix in development. *Development* **147** (2020).
19. Halbleib, J.M. & Nelson, W.J. Cadherins in development: cell adhesion, sorting, and tissue morphogenesis. *Genes Dev* **20**, 3199-3214 (2006).
20. Foty, R.A. & Steinberg, M.S. The differential adhesion hypothesis: a direct evaluation. *Dev Biol* **278**, 255-263 (2005).
21. Hogan, C. *et al.* Rap1 Regulates the Formation of E-Cadherin-Based Cell-Cell Contacts. *Molecular and Cellular Biology* **24**, 6690-6700 (2004).
22. Johnson, E., Theisen, C.S., Johnson, K.R. & Wheelock, M.J. R-cadherin influences cell motility via Rho family GTPases. *J Biol Chem* **279**, 31041-31049 (2004).

23. Luo, J., Treubert-Zimmermann, U. & Redies, C. Cadherins guide migrating Purkinje cells to specific parasagittal domains during cerebellar development. *Mol Cell Neurosci* **25**, 138-152 (2004).
24. Maeda, M., Johnson, K.R. & Wheelock, M.J. Cadherin switching: essential for behavioral but not morphological changes during an epithelium-to-mesenchyme transition. *J Cell Sci* **118**, 873-887 (2005).
25. Reintsch, W.E., Habring-Mueller, A., Wang, R.W., Schohl, A. & Fagotto, F. beta-Catenin controls cell sorting at the notochord-somite boundary independently of cadherin-mediated adhesion. *J Cell Biol* **170**, 675-686 (2005).
26. Takahashi, K. *et al.* Induction of pluripotent stem cells from adult human fibroblasts by defined factors. *Cell* **131**, 861-872 (2007).
27. Takahashi, K. & Yamanaka, S. Induction of pluripotent stem cells from mouse embryonic and adult fibroblast cultures by defined factors. *Cell* **126**, 663-676 (2006).
28. Bao, X. *et al.* Long-term self-renewing human epicardial cells generated from pluripotent stem cells under defined xeno-free conditions. *Nat Biomed Eng* **1** (2016).
29. Bax, N.A.M. *et al.* In vitro epithelial-to-mesenchymal transformation in human adult epicardial cells is regulated by TGFβ-signaling and WT1. *Basic Res Cardiol* **106**, 829-847 (2011).
30. Burridge, P.W., Keller, G., Gold, J.D. & Wu, J.C. Production of de novo cardiomyocytes: human pluripotent stem cell differentiation and direct reprogramming. *Cell Stem Cell* **10**, 16-28 (2012).
31. Compton, L.A., Potash, D.A., Mundell, N.A. & Barnett, J.V. Transforming growth factor-β induces loss of epithelial character and smooth muscle cell differentiation in epicardial cells. *Developmental Dynamics* **235**, 82-93 (2006).
32. Iyer, D. *et al.* Robust derivation of epicardium and its differentiated smooth muscle cell progeny from human pluripotent stem cells. *Development* **142**, 1528-1541 (2015).
33. Mummery, C.L. *et al.* Differentiation of human embryonic stem cells and induced pluripotent stem cells to cardiomyocytes: a methods overview. *Circ Res* **111**, 344-358 (2012).
34. Tuyn, J.v. *et al.* Epicardial Cells of Human Adults Can Undergo an Epithelial-to-Mesenchymal Transition and Obtain Characteristics of Smooth Muscle Cells In Vitro. *STEM CELLS* **25**, 271-278 (2007).
35. Witty, A.D. *et al.* Generation of the epicardial lineage from human pluripotent stem cells. *Nat Biotechnol* **32**, 1026-1035 (2014).
36. Zhao, J. *et al.* Efficient Differentiation of TBX18(+)/WT1(+) Epicardial-Like Cells from Human Pluripotent Stem Cells Using Small Molecular Compounds. *Stem Cells Dev* **26**, 528-540 (2017).
37. Watt, A.J., Battle, M.A., Li, J. & Duncan, S.A. GATA4 is essential for formation of the proepicardium and regulates cardiogenesis. *Proc Natl Acad Sci U S A* **101**, 12573-12578 (2004).
38. Bai, Y.H. *et al.* A Novel Tumor-Suppressor, CDH18, Inhibits Glioma Cell Invasiveness Via UQCRC2 and Correlates with the Prognosis of Glioma Patients. *Cell Physiol Biochem* **48**, 1755-1770 (2018).
39. Klein, M.E. *et al.* PDLIM7 and CDH18 regulate the turnover of MDM2 during CDK4/6 inhibitor therapy-induced senescence. *Oncogene* **37**, 5066-5078 (2018).
40. Shibata, T., Shimoyama, Y., Gotoh, M. & Hirohashi, S. Identification of human cadherin-14, a novel neurally specific type II cadherin, by protein interaction cloning. *J Biol Chem* **272**, 5236-5240 (1997).
41. Funakoshi, S. *et al.* Enhanced engraftment, proliferation, and therapeutic potential in heart using optimized human iPSC-derived cardiomyocytes. *Sci Rep* **6**, 19111 (2016).
42. Yang, J. *et al.* Guidelines and definitions for research on epithelial-mesenchymal transition. *Nat Rev Mol Cell Biol* **21**, 341-352 (2020).

43. Moerkamp, A.T. *et al.* Human fetal and adult epicardial-derived cells: a novel model to study their activation. *Stem Cell Res Ther* **7**, 174 (2016).
44. Wei, X. *et al.* Biological characteristics of embryonic epicardial cells in vitro correlate with embryonic day. *Acta Biochim Biophys Sin (Shanghai)* **49**, 14-24 (2017).
45. Dokic, D. & Dettman, R.W. VCAM-1 inhibits TGFβ stimulated epithelial–mesenchymal transformation by modulating Rho activity and stabilizing intercellular adhesion in epicardial mesothelial cells. *Dev. Biol.* **299**, 489-504 (2006).
46. Dronkers, E., Wauters, M.M.M., Goumans, M.J. & Smits, A.M. Epicardial TGFβ and BMP Signaling in Cardiac Regeneration: What Lesson Can We Learn from the Developing Heart? *Biomolecules* **10**, 404 (2020).
47. Goumans, M.-J. & Ten Dijke, P. TGF-β Signaling in Control of Cardiovascular Function. *Cold Spring Harbor Perspectives in Biology* **10** (2018).
48. Hill, C.R. *et al.* BMP2 signals loss of epithelial character in epicardial cells but requires the Type III TGFβ receptor to promote invasion. *Cellular Signalling* **24**, 1012-1022 (2012).
49. Ishii, Y., Garriock, R.J., Navetta, A.M., Coughlin, L.E. & Mikawa, T. BMP Signals Promote Proepicardial Protrusion Necessary for Recruitment of Coronary Vessel and Epicardial Progenitors to the Heart. *Dev. Cell* **19**, 307-316 (2010).
50. Lu, J. *et al.* Coronary smooth muscle differentiation from proepicardial cells requires rhoA-mediated actin reorganization and p160 rho-kinase activity. *Dev. Biol.* **240**, 404-418 (2001).
51. Mack, C.P. Signaling mechanisms that regulate smooth muscle cell differentiation. *Arterioscler Thromb Vasc Biol* **31**, 1495-1505 (2011).
52. Rudat, C., Norden, J., Taketo, M.M. & Kispert, A. Epicardial function of canonical Wnt-, Hedgehog-, Fgfr1/2-, and Pdgfra-signalling. *Cardiovascular Research* **100**, 411-421 (2013).
53. Smith, C.L., Baek, S.T., Sung, C.Y. & Tallquist, M.D. Epicardial-derived cell epithelial-to-mesenchymal transition and fate specification require PDGF receptor signaling. *Circulation Research* **108**, e15-26 (2011).
54. Zhou, B.P. *et al.* Dual regulation of Snail by GSK-3beta-mediated phosphorylation in control of epithelial-mesenchymal transition. *Nat Cell Biol* **6**, 931-940 (2004).
55. Duan, J. *et al.* Wnt1/betacatenin injury response activates the epicardium and cardiac fibroblasts to promote cardiac repair. *EMBO J* **31**, 429-442 (2012).
56. Heuberger, J. & Birchmeier, W. Interplay of cadherin-mediated cell adhesion and canonical Wnt signaling. *Cold Spring Harb Perspect Biol* **2**, a002915 (2010).
57. Nelson, W.J. & Nusse, R. Convergence of Wnt, beta-catenin, and cadherin pathways. *Science* **303**, 1483-1487 (2004).
58. Shimoyama, Y., Takeda, H., Yoshihara, S., Kitajima, M. & Hirohashi, S. Biochemical characterization and functional analysis of two type II classic cadherins, cadherin-6 and -14, and comparison with E-cadherin. *J Biol Chem* **274**, 11987-11994 (1999).
59. Acharya, A. *et al.* The bHLH transcription factor Tcf21 is required for lineage-specific EMT of cardiac fibroblast progenitors. *Development* **139**, 2139-2149 (2012).
60. Braitsch, C.M., Combs, M.D., Quaggin, S.E. & Yutzey, K.E. Pod1/Tcf21 is regulated by retinoic acid signaling and inhibits differentiation of epicardium-derived cells into smooth muscle in the developing heart. *Dev. Biol.* **368**, 345-357 (2012).
61. Hu, H., Lin, S., Wang, S. & Chen, X. The Role of Transcription Factor 21 in Epicardial Cell Differentiation and the Development of Coronary Heart Disease. *Front Cell Dev Biol* **8**, 457 (2020).
62. Lupu, I.E., De Val, S. & Smart, N. Coronary vessel formation in development and disease: mechanisms and insights for therapy. *Nat Rev Cardiol* **17**, 790-806 (2020).

63. Tevosian, S.G. *et al.* FOG-2, a cofactor for GATA transcription factors, is essential for heart morphogenesis and development of coronary vessels from epicardium. *Cell* **101**, 729-739 (2000).
64. Zhuge, Y. *et al.* Role of smooth muscle cells in Cardiovascular Disease. *Int J Biol Sci* **16**, 2741-2751 (2020).
65. Wu, M. *et al.* Epicardial spindle orientation controls cell entry into the myocardium. *Dev. Cell* **19**, 114-125 (2010).
66. Risebro, C.A., Vieira, J.M., Klotz, L. & Riley, P.R. Characterisation of the human embryonic and foetal epicardium during heart development. *Development* **142**, 3630-3636 (2015).
67. Velecela, V. *et al.* Epicardial cell shape and maturation are regulated by Wt1 via transcriptional control of Bmp4. *Development* **146** (2019).
68. Meigs, T.E., Fields, T.A., McKee, D.D. & Casey, P.J. Interaction of Gα12 and Gα13 with the cytoplasmic domain of cadherin provides a mechanism for β-catenin release. *PNAS* **98**, 519-524 (2001).
69. Rudat, C. & Kispert, A. Wt1 and Epicardial Fate Mapping. *Circulation Research* **111**, 165-169 (2012).
70. Zamora, M., Männer, J. & Ruiz-Lozano, P. Epicardium-derived progenitor cells require β-catenin for coronary artery formation. *PNAS* **104**, 18109-18114 (2007).
71. Azambuja Ana, P. *et al.* Retinoic Acid and VEGF Delay Smooth Muscle Relative to Endothelial Differentiation to Coordinate Inner and Outer Coronary Vessel Wall Morphogenesis. *Circulation Research* **107**, 204-216 (2010).
72. Guadix, J.A. *et al.* Wt1 controls retinoic acid signalling in embryonic epicardium through transcriptional activation of Raldh2. *Development* **138**, 1093-1097 (2011).
73. Sridurongrit, S., Larsson, J., Schwartz, R., Ruiz-Lozano, P. & Kaartinen, V. Signaling via the Tgf-beta type I receptor Alk5 in heart development. *Dev. Biol.* **322**, 208-218 (2008).
74. Sánchez, N.S. & Barnett, J.V. TGFβ and BMP-2 regulate epicardial cell invasion via TGFβR3 activation of the Par6/Smurf1/RhoA pathway. *Cellular Signalling* **24**, 539-548 (2012).
75. Zhao, W. *et al.* Effect of TGF-β1 on the Migration and Recruitment of Mesenchymal Stem Cells after Vascular Balloon Injury: Involvement of Matrix Metalloproteinase-14. *Scientific Reports* **6**, 21176 (2016).
76. Tao, J., Barnett, J.V., Watanabe, M. & Ramírez-Bergeron, D. Hypoxia Supports Epicardial Cell Differentiation in Vascular Smooth Muscle Cells through the Activation of the TGFβ Pathway. *Journal of Cardiovascular Development and Disease* **5** (2018).

Figure 1

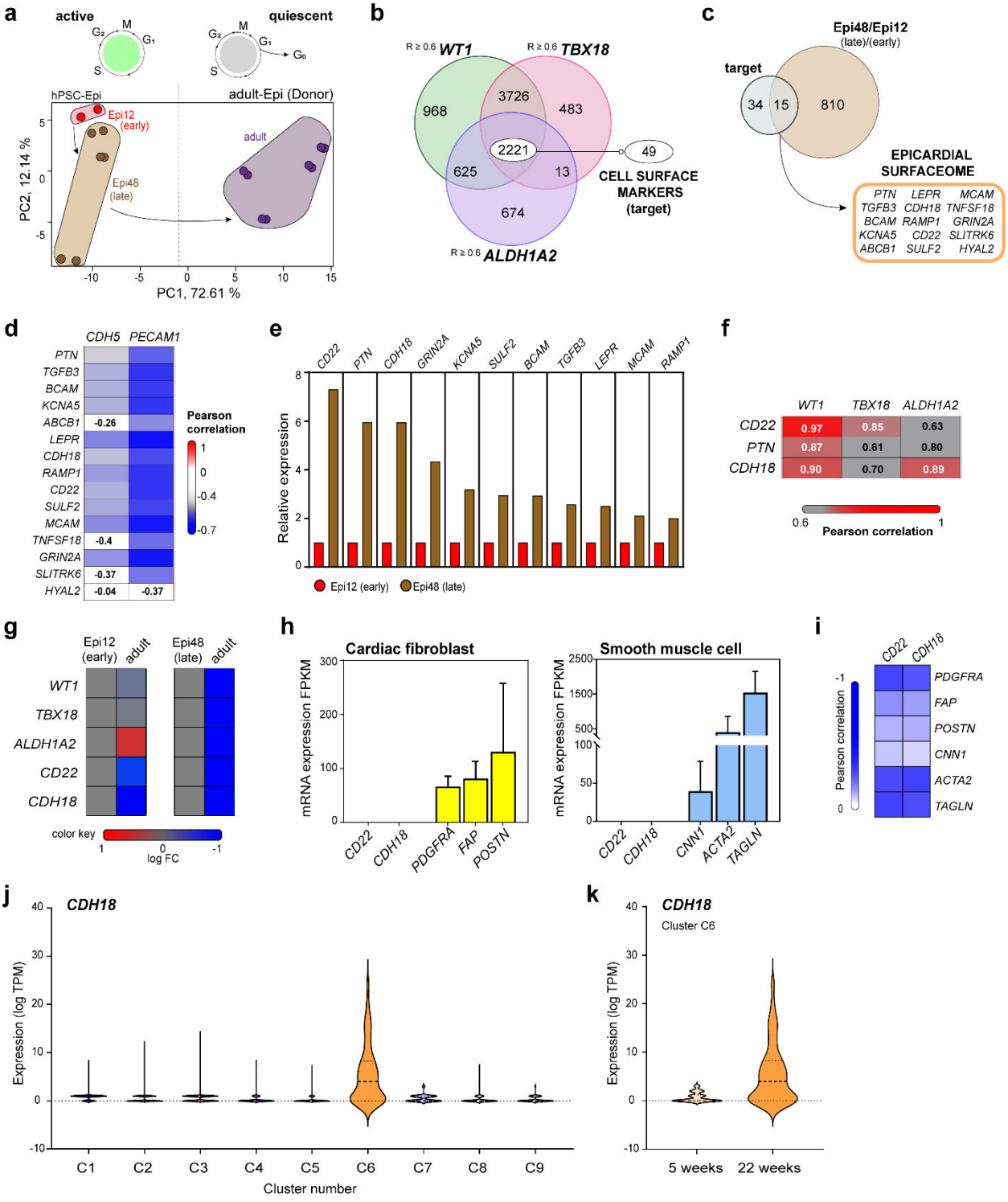
a
active
quiescent
hPSC-Epi
adult-Epi (Donor)
Epi12 (early)
Epi48 (late)
adult
PC2, 12.14 %
PC1, 72.61 %
b
R ≥ 0.6 WT1
R ≥ 0.6 TBX18
R ≥ 0.6 ALDH1A2
968
3726
483
2221
49
625
13
674
CELL SURFACE MARKERS (target)
c
Epi48/Epi12 (late)/(early)
target
34
15
810
EPICARDIAL SURFACEOME
PTN LEPR MCAM
TGFB3 CDH18 TNFSF18
BCAM RAMP1 GRIN2A
KCNA5 CD22 SLITRK6
ABCB1 SULF2 HYAL2
d
CDH5 PECAM1
PTN
TGFB3
BCAM
KCNA5
ABCB1 -0.26
LEPR
CDH18
RAMP1
CD22
SULF2
MCAM
TNFSF18 -0.4
GRIN2A
SLITRK6 -0.37
HYAL2 -0.04 -0.37
Pearson correlation
1
0
-0.4
-0.7
e
CD22 PTN CDH18 GRIN2A KCNA5 SULF2 BCAM TGFB3 LEPR MCAM RAMP1
Relative expression
Epi12 (early)
Epi48 (late)
f
WT1 TBX18 ALDH1A2
CD22 0.97 0.85 0.63
PTN 0.87 0.61 0.80
CDH18 0.90 0.70 0.89
0.6
Pearson correlation
1
g
Epi12 (early)
adult
Epi48 (late)
adult
WT1
TBX18
ALDH1A2
CD22
CDH18
color key
log FC
h
Cardiac fibroblast
mRNA expression FPKM
CD22 CDH18 PDGFRA FAP POSTN
Smooth muscle cell
mRNA expression FPKM
CD22 CDH18 CNN1 ACTA2 TAGLN
i
CD22 CDH18
Pearson correlation
PDGFRA
FAP
POSTN
CNN1
ACTA2
TAGLN
j
CDH18
Expression (log TPM)
C1 C2 C3 C4 C5 C6 C7 C8 C9
Cluster number
k
CDH18
Cluster C6
Expression (log TPM)
5 weeks
22 weeks

Figure 2

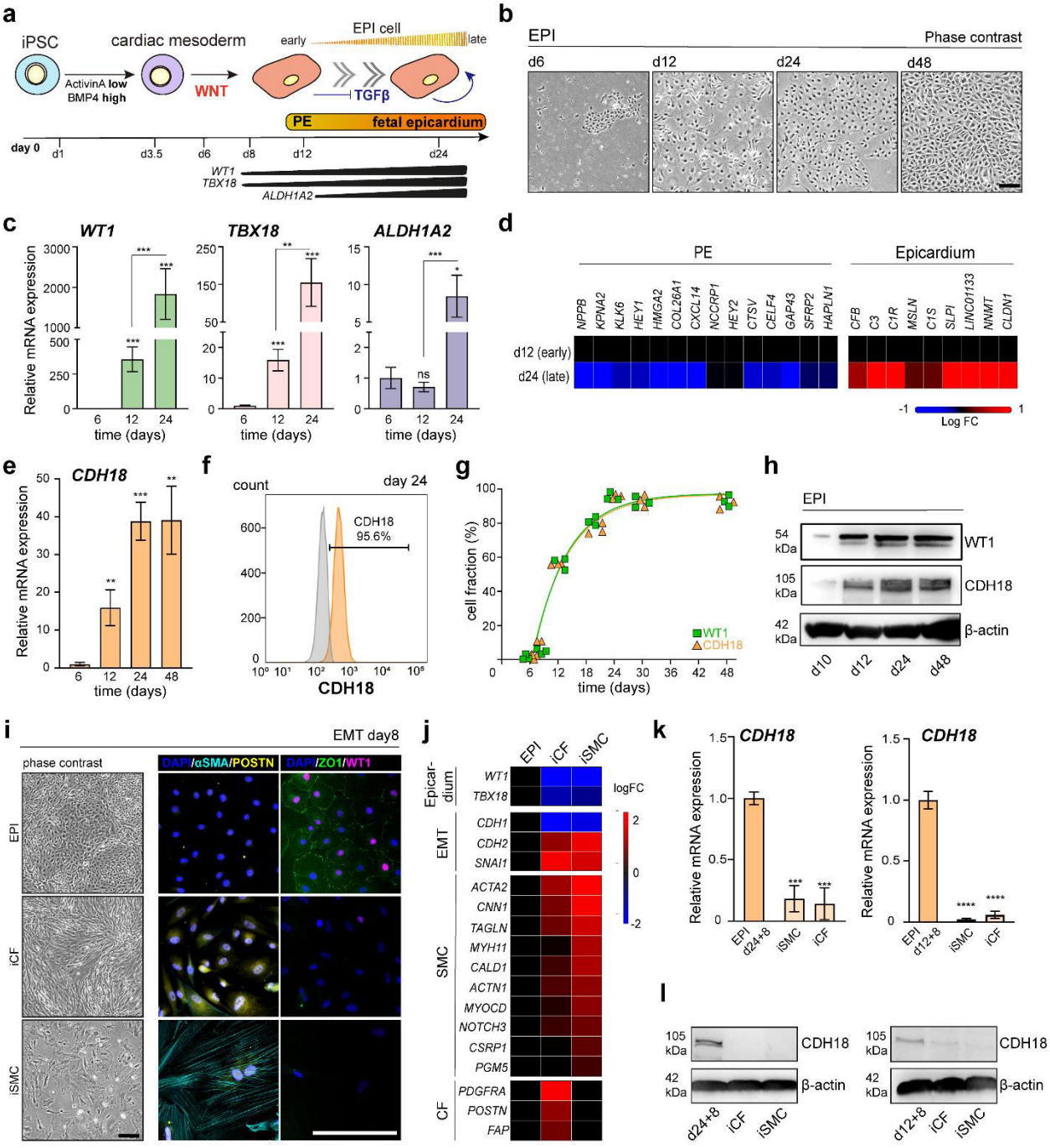
a
iPSC
cardiac mesoderm
EPI cell
early
late
ActivinA low
BMP4 high
WNT
TGFβ
PE
fetal epicardium
day 0
d1
d3.5
d6
d8
d12
d24
WT1
TBX18
ALDH1A2
b
EPI
Phase contrast
d6
d12
d24
d48
c
WT1
TBX18
ALDH1A2
Relative mRNA expression
time (days)
ns
d
PE
Epicardium
NPPB
KPNA2
KLK6
HEY1
HMGA2
COL26A1
CXCL14
NCCRP1
HEY2
CTSV
CELF4
GAP43
SFRP2
HAPLN1
CFB
C3
C1R
MSLN
C1S
SLPI
LINC01133
NNMT
CLDN1
d12 (early)
d24 (late)
Log FC
e
CDH18
Relative mRNA expression
time (days)
f
count
day 24
CDH18
95.6%
CDH18
g
cell fraction (%)
time (days)
WT1
CDH18
h
EPI
54 kDa
WT1
105 kDa
CDH18
42 kDa
β-actin
d10
d12
d24
d48
i
EMT day8
phase contrast
DAPI/αSMA/POSTN
DAPI/ZO1/WT1
EPI
iCF
iSMC
j
EPI
iCF
iSMC
Epicar-dium
WT1
TBX18
EMT
CDH1
CDH2
SNAI1
SMC
ACTA2
CNN1
TAGLN
MYH11
CALD1
ACTN1
MYOCD
NOTCH3
CSRP1
PGM5
CF
PDGFRA
POSTN
FAP
logFC
k
CDH18
Relative mRNA expression
EPI
d24+8
iSMC
iCF
CDH18
Relative mRNA expression
EPI
d12+8
iSMC
iCF
l
105 kDa
CDH18
42 kDa
β-actin
d24+8
iCF
iSMC
105 kDa
CDH18
42 kDa
β-actin
d12+8
iCF
iSMC

Figure 3

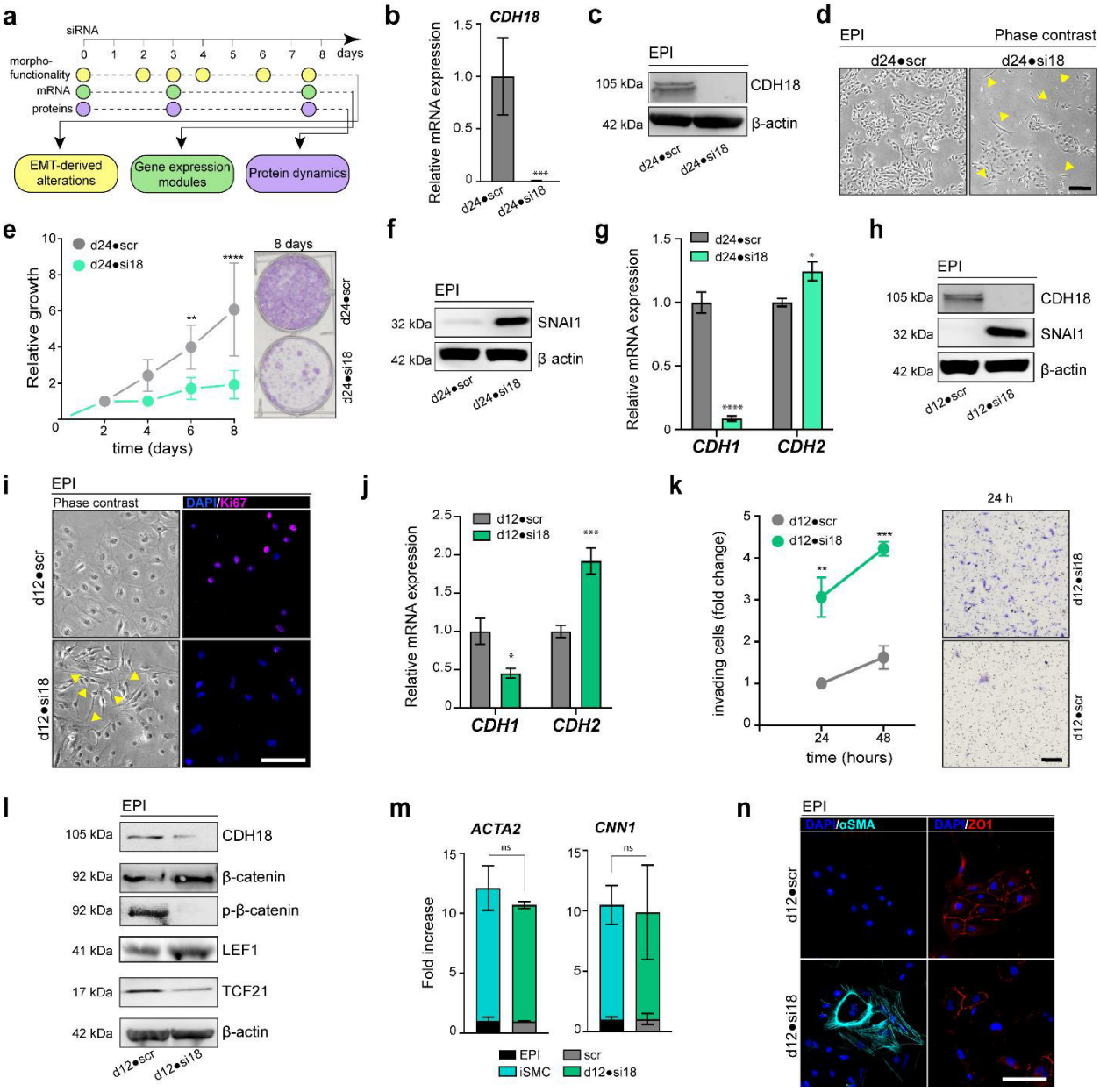
a
siRNA
0 1 2 3 4 5 6 7 8 days
morpho-functionality
mRNA
proteins
EMT-derived alterations
Gene expression modules
Protein dynamics
b
CDH18
Relative mRNA expression
d24•scr
d24•si18
c
EPI
105 kDa
CDH18
42 kDa
β-actin
d
EPI
Phase contrast
d24•scr
d24•si18
e
d24•scr
d24•si18
Relative growth
time (days)
8 days
f
EPI
32 kDa
SNAI1
42 kDa
β-actin
g
Relative mRNA expression
CDH1
CDH2
h
EPI
105 kDa
CDH18
32 kDa
SNAI1
42 kDa
β-actin
d12•scr
d12•si18
i
EPI
Phase contrast
DAPI/Ki67
d12•scr
d12•si18
j
Relative mRNA expression
CDH1
CDH2
k
invading cells (fold change)
time (hours)
24 h
l
EPI
105 kDa
CDH18
92 kDa
β-catenin
92 kDa
p-β-catenin
41 kDa
LEF1
17 kDa
TCF21
42 kDa
β-actin
m
ACTA2
CNN1
Fold increase
ns
EPI
iSMC
scr
d12•si18
n
EPI
DAPI/αSMA
DAPI/ZO1
d12•scr
d12•si18

Figure 4

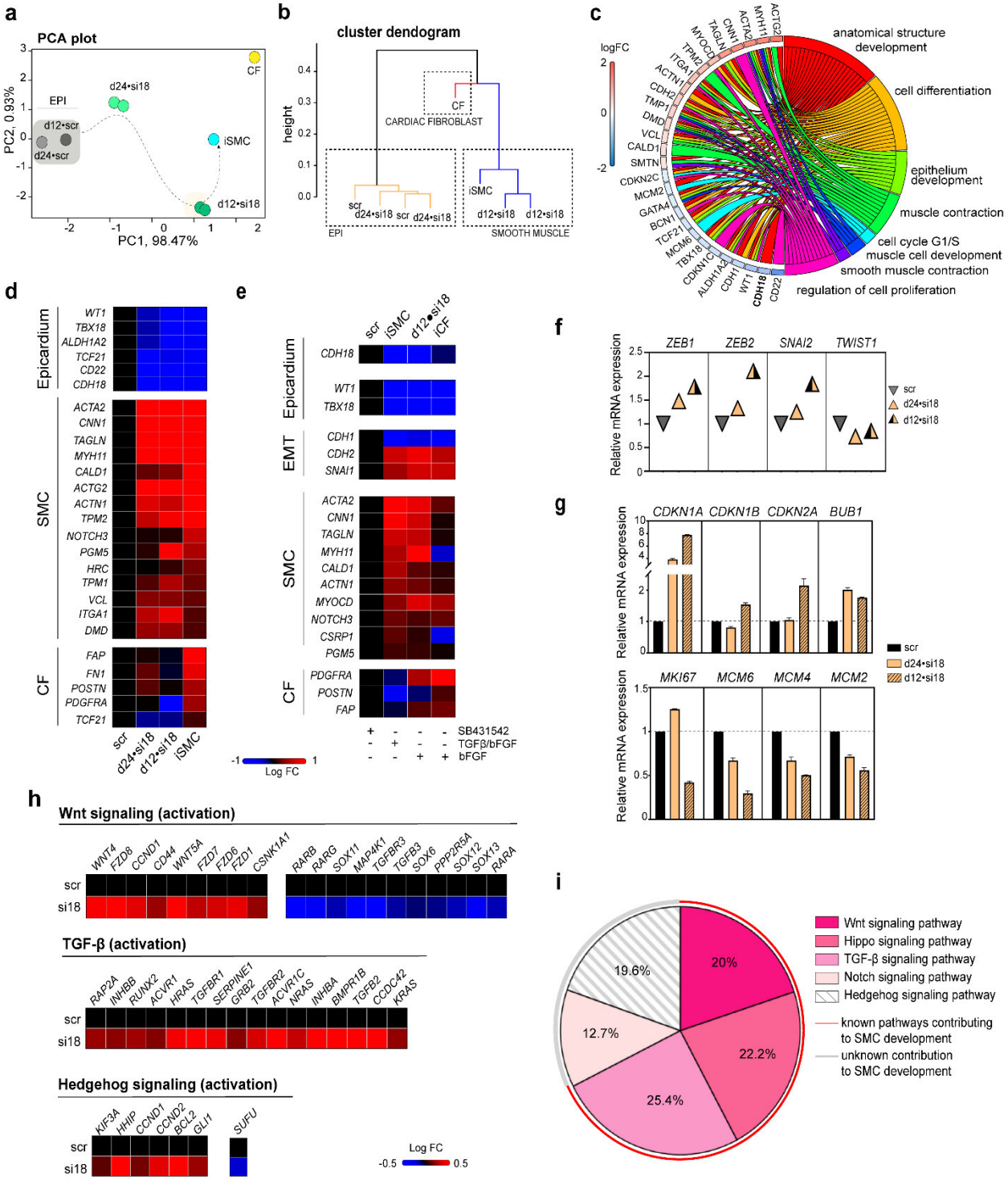
a
PCA plot
PC2, 0.93%
PC1, 98.47%
EPI
d12•scr
d24•scr
d24•si18
CF
iSMC
d12•si18
b
cluster dendogram
height
CF
CARDIAC FIBROBLAST
iSMC
scr
d24•si18
d12•si18
EPI
SMOOTH MUSCLE
c
logFC
anatomical structure development
cell differentiation
epithelium development
muscle contraction
cell cycle G1/S
muscle cell development
smooth muscle contraction
regulation of cell proliferation
d
Epicardium
SMC
CF
WT1
TBX18
ALDH1A2
TCF21
CD22
CDH18
ACTA2
CNN1
TAGLN
MYH11
CALD1
ACTG2
ACTN1
TPM2
NOTCH3
PGM5
HRC
TPM1
VCL
ITGA1
DMD
FAP
FN1
POSTN
PDGFRA
TCF21
scr
d24•si18
d12•si18
iSMC
Log FC
e
scr
iSMC
d12•si18
iCF
Epicardium
CDH18
WT1
TBX18
EMT
CDH1
CDH2
SNAI1
SMC
ACTA2
CNN1
TAGLN
MYH11
CALD1
ACTN1
MYOCD
NOTCH3
CSRP1
PGM5
CF
PDGFRA
POSTN
FAP
SB431542
TGFβ/bFGF
bFGF
Log FC
f
ZEB1
ZEB2
SNAI2
TWIST1
Relative mRNA expression
scr
d24•si18
d12•si18
g
CDKN1A
CDKN1B
CDKN2A
BUB1
MKI67
MCM6
MCM4
MCM2
Relative mRNA expression
scr
d24•si18
d12•si18
h
Wnt signaling (activation)
WNT4
FZD8
CCND1
CD44
WNT5A
FZD7
FZD6
FZD1
CSNK1A1
RARB
RARG
SOX11
MAP4K1
TGFBR3
TGFB3
SOX6
PPP2R5A
SOX12
SOX13
RARA
scr
si18
TGF-β (activation)
RAP2A
INHBB
RUNX2
ACVR1
HRAS
TGFBR1
SERPINE1
GRB2
TGFBR2
ACVR1C
NRAS
INHBA
BMPR1B
TGFB2
CCDC42
KRAS
scr
si18
Hedgehog signaling (activation)
KIF3A
HHIP
CCND1
CCND2
BCL2
GLI1
SUFU
scr
si18
Log FC
-0.5
0.5
i
20%
22.2%
25.4%
12.7%
19.6%
Wnt signaling pathway
Hippo signaling pathway
TGF-β signaling pathway
Notch signaling pathway
Hedgehog signaling pathway
known pathways contributing to SMC development
unknown contribution to SMC development

Figure 5

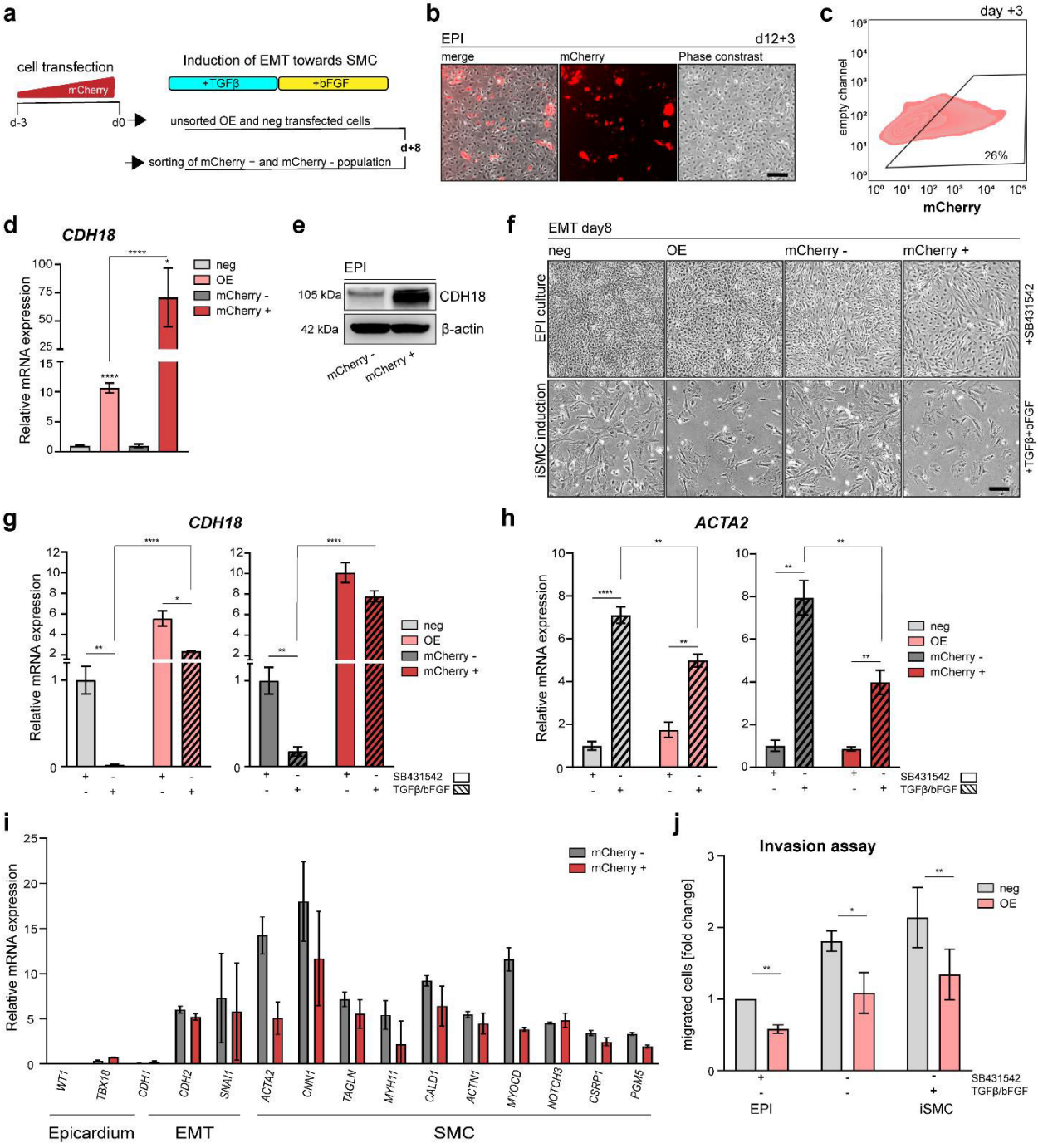
a
cell transfection
mCherry
d-3
d0
Induction of EMT towards SMC
+TGFβ
+bFGF
unsorted OE and neg transfected cells
d+8
sorting of mCherry + and mCherry - population
b
EPI
d12+3
merge
mCherry
Phase constrast
c
day +3
empty channel
26%
mCherry
d
CDH18
Relative mRNA expression
neg
OE
mCherry -
mCherry +
e
EPI
105 kDa
CDH18
42 kDa
β-actin
mCherry -
mCherry +
f
EMT day8
neg
OE
mCherry -
mCherry +
EPI culture
iSMC induction
+SB431542
+TGFβ+bFGF
g
CDH18
Relative mRNA expression
SB431542
TGFβ/bFGF
h
ACTA2
Relative mRNA expression
SB431542
TGFβ/bFGF
i
Relative mRNA expression
mCherry -
mCherry +
WT1
TBX18
CDH1
CDH2
SNAI1
ACTA2
CNN1
TAGLN
MYH11
CALD1
ACTN1
MYOCD
NOTCH3
CSRP1
PGM5
Epicardium
EMT
SMC
j
Invasion assay
migrated cells [fold change]
neg
OE
SB431542
TGFβ/bFGF
EPI
iSMC

Figure 6

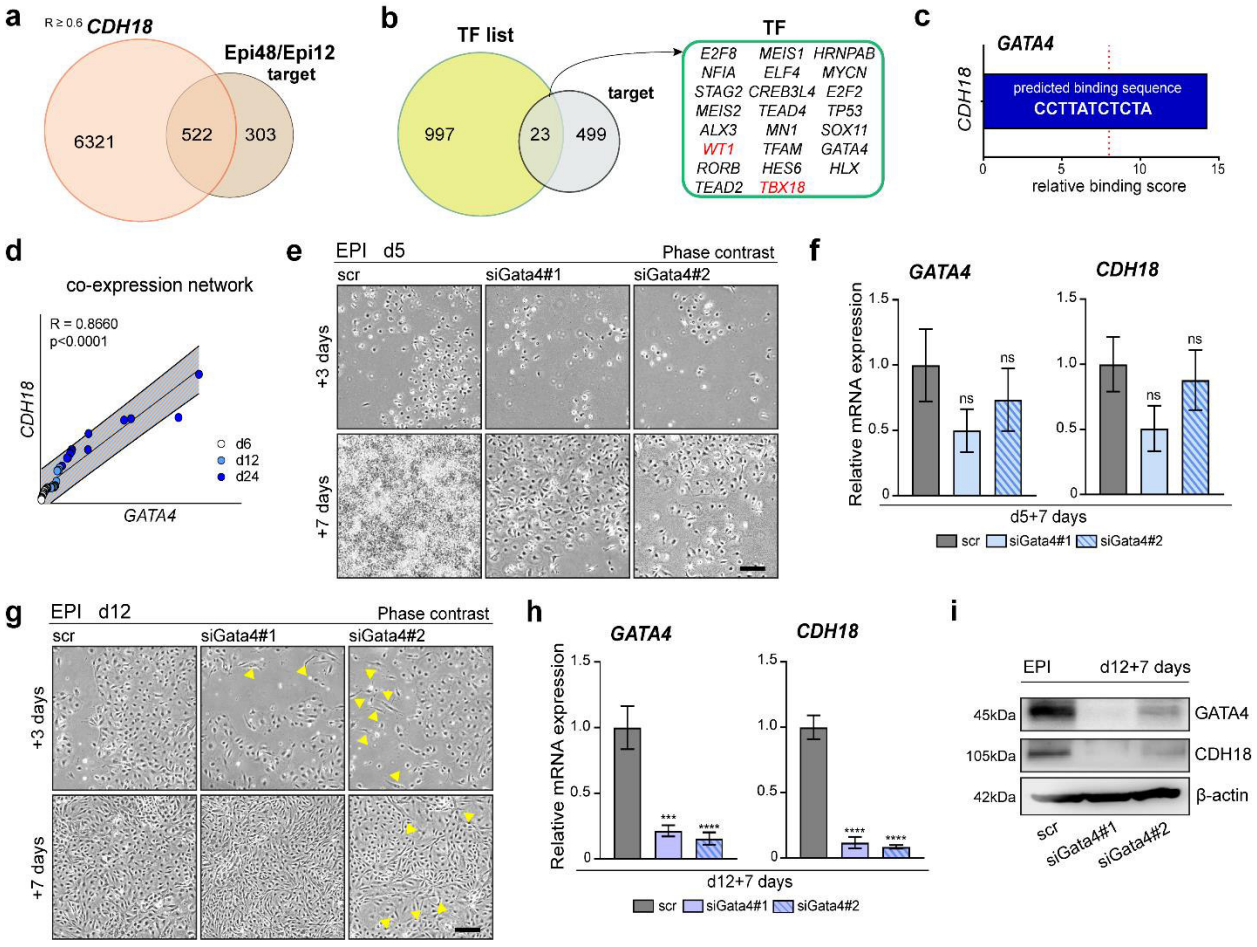
a
R ≥ 0.6 CDH18
Epi48/Epi12 target
6321
522
303
b
TF list
target
997
23
499
TF
E2F8 MEIS1 HRNPAB
NFIA ELF4 MYCN
STAG2 CREB3L4 E2F2
MEIS2 TEAD4 TP53
ALX3 MN1 SOX11
WT1 TFAM GATA4
RORB HES6 HLX
TEAD2 TBX18
c
GATA4
CDH18
predicted binding sequence
CCTTATCTCTA
0 5 10 15
relative binding score
d
co-expression network
R = 0.8660
p<0.0001
CDH18
GATA4
d6
d12
d24
e
EPI d5
Phase contrast
scr
siGata4#1
siGata4#2
+3 days
+7 days
f
GATA4
CDH18
Relative mRNA expression
1.5
1.0
0.5
0
ns
d5+7 days
scr siGata4#1 siGata4#2
g
EPI d12
Phase contrast
scr
siGata4#1
siGata4#2
+3 days
+7 days
h
GATA4
CDH18
Relative mRNA expression
***
****
d12+7 days
scr siGata4#1 siGata4#2
i
EPI
d12+7 days
45kDa
105kDa
42kDa
GATA4
CDH18
β-actin
scr
siGata4#1
siGata4#2

FIGURE LEGENDS

Figure 1. Defined surfaceome transcript of the developing epicardium revealed the enrichment of *CD22* and *CDH18* in late-stage populations

a, PCA using the GSE84085 RNA-Seq expression dataset of d12 early epicardial-like cells (Epi12, red) (19-9-7-Epi, n=2), d48 late epicardial-like cells (Epi48, brown) (H9-Epi, ES03-Epi and 19-9-11-Epi, n=6) and human adult epicardium (dark violet) (donors 9605, 9633, 9634 and 9635, n=8). **b,** Venn-Diagram showing genes in significant absolute correlation to the epicardial markers *WT1* (light green), *TBX18* (light pink) and *ALDH1A2* (light purple) (Pearson correlations; R ≥ 0.6) as well as cell surface marker enrichment (target)**. c,** Overlap of the target gene set from (**b**) (grey) against DEGs (Supplementary Figure 1e) (light brown) for the surfaceome transcript identification of the epicardium. **d**, Heatmap showing correlations (Pearson, R, 1 – -0.7, color scale) of surface marker expression relative to the expression of endothelial cell markers *CDH5* and *PECAM1*. **e,** Fold change of surface marker expression in Epi48 (brown) relative to Epi12 (red). **f,** Heatmap showing correlations (Pearson, R, 0.6 – 1, color scale) of the top three genes from (**e**) to epicardial markers. **g,** Retrospective analysis showing a heatmap depicting active epicardial markers and *CD22* and *CDH18* expression in embryonic and adult cells. **h,** Analysis for *CD22* and *CDH18* expression in CF (left) and SMC (right) with representative CF genes (yellow) and SMC genes (light blue). [Error bars indicate standard derivation (SD)]. **i,** Heatmap showing correlations (Pearson, R, 0 – -1, color scale) of *CD22* and *CDH18* for CF markers *PDGFRA*, *FAP* and *POSTN* and SMC markers *CNN1*, *ACTA2*, and *TAGLN*. **j**, GSE106168 retrospective analysis for *CDH18* expression in different cardiac cellular clusters [(C1 - 5W whole heart (n=257); C2 - Cardiomyocytes (n=1492); C3 - fibroblast-like cells (n=786); C4 – Endothelial cells (n=445); C5 - Heart valves (n=427); C6 – Epicardial -EPI- cells (n=46); C7 - immune cells (n=27); C8 - macrophages (n=308); C9 - T and B lymphocytes (n=58)] **k,** GSE106168 retrospective analysis for *CDH18* expression in epicardial -EPI- cluster [*UPK3B*^{high} *WT1*^{high} *TBX18*^{high} *ALDH1A2*^{high}] ranging different time points of gestation [5 weeks, n=30; 22 weeks, n=46].

Figure 2 CDH18 but not CD22 is an epicardial biomarker defining progressive lineage specification

a, Schematic illustration depicting the epicardial differentiation from hiPSCs and representative developmental stages. **b**, Phase contrast microscopy showing the morphology of EPI cells from d6-48. **c**, qRT-PCR analysis of *WT1* (light green), *TBX18* (light red) and *ALDH1A2* (light purple) during induction normalized to d6. [d6 n=7, d12 n=10, d24 n=10; * $p<0.05$, ** $p<0.005$, *** $p<0.0005$]. **d**, Heatmap showing PE and primitive epicardium gene signature enriched in d12 and d24 EPI cells respectively. **e**, Time course of *CDH18* expression levels (orange) normalized to d6. [d6 n=4, d12 n=4, d24 n=8, d48 n=8; ** $p<0.01$, *** $p=0.0008$]. **f**, Flow cytometry analysis for CDH18 (orange) [grey, unstained control]. **g**, Nonlinear-regression fit curve depicting WT1 (green, squares) and CDH18 (orange, triangles) co-expression in EPI cells [n=3]. **h**, Western blot analysis showing the co-expression of WT1 and CDH18 in EPI cells during induction. **i**, Immunocytochemistry of the EPDC markers POSTN (CF) and αSMA (SMC) and the EPI markers ZO1 and WT1 for EMT validation [fluorescence microscopy images were pseudo-colored using BZ-X analyzer software]. **j,** Heatmap of epicardium, EMT, SMC and CF gene signatures [GSE165450]. **k-l**, *CDH18* expression analyzed by (**k**) qRT-PCR in induced derivatives (light orange) from d24 cells (left) and d12 cells (right), normalized to the respective EPI control cells (orange) [n=3; one-way ANOVA with Dunnett's multiple comparison test, *** $p<0.0005$] with (**l**) corresponding western blot analysis.
[statistical analysis performed by Mann-Whitney-test, unless otherwise indicated; all error bars represent standard error of the mean (SEM); scale bars 100µm].

Figure 3 Loss of *CDH18* triggers cell-fate specific EMT towards smooth muscle cells

a, Illustration of the experimental workflow. **b-c**, Downregulation of (**b**) *CDH18* [n=3; unpaired students t-test, *** p=0.0003] and (**c**) CDH18 protein expression after 8 days of *CDH18* silencing in d24 EPI cells (d24•si18). **d**, Phase contrast microscopy displaying d24•si18 cells with lost cobblestone morphology and elongated shape (yellow arrowheads). **e**, Growth curve of d24 cells silenced for *CDH18* (green) and control (scr) (grey) for 2-8 days [n=3; ** p=0.0038, **** p<0.0001]. **f,** SNAI1 western blot of d24•si18 cells. **g,** *CDH1* and *CDH2* expression in d24•si18 cells [control (scr); n=3; * p=0.0141, **** p<0.0001]. **h**, Western blot of CDH18 and SNAI1 after 8 days of *CDH18* silencing in d24 EPI cells (d12•si18). **i**, Microscopy analysis of d12•si18 showing changed morphology (yellow arrowheads) and loss of Ki67 (pink) expression [scale bar 50µm]. **j**, Expression of *CDH1* and *CDH2* in d12•si18 EPI cells compared to their control cells. [n=3; * p=0.0231, *** p=0.0001]. **k**, Boyden chamber assay evaluating cell migration capacity in d12•si18 cells [n=3; ** p=0.002, *** p=0.0004]. Right panel shows invaded cells stained by crystal violet. **l**, Western blot analysis showing reduction of CDH18 and TCF21, increased LEF1 and β-catenin with decreased phosphorylated (p)-β-catenin. **m**, Expression analysis of SMC markers *ACTA2* and *CNN1* in d12•si18 cells and iSMC [n=3; unpaired students t-test: ns = not significant]. **n,** Immunocytochemistry analysis of αSMA and ZO1 expression in d12•si18 cells [scale bar 50µm].

[statistical analysis performed by two-way ANOVA with Sidak's multiple comparison test, unless otherwise indicated; all error bars represent SEM; scale bars 100µm, unless otherwise indicated].

Figure 4. Transcriptional profiling of *CDH18*-silenced EPI cells

a, PCA of *CDH18*-silenced d12 and d24 EPI cells as well as induced EPDCs compared to unspecific siRNA-treated control (scr) [d24•si18, n=2; d12•si18, n=2; iSMC, n=1; CF; n=1]. **b,** Agglomerative hierarchical sample cluster: The Agnes dendrogram was plotted by applying Manhattan distances between samples. **c,** Chord diagram representing flow and detailed relationship between d12•si18 DEGs (left semicircle perimeter) and their enriched GO biological processes (right semicircle perimeter). **d,** Heatmap showing the expression analysis of the gene set enriched for epicardial, SMC and CF genes in iSMCs, *CDH18*-downregulated and control (scr) cells. **e,** Heatmap showing the expression analysis of the gene set enriched for epicardial, SMC and CF genes in *CDH18*-downregulated and control (scr) cells under different culture conditions. **f-g,** Expression levels for (**f**) EMT specific transcription factors (EMT-TFs) *ZEB1*, *ZEB2*, *SNAI2* and *TWIST1* and (**g**) *CDKN1A*, *CDKN1B*, *CDKN2A*, *BUB1*, *MKI67*, *MCM6*, *MCM4* and *MCM2* in *CDH18*-downregulated cells. **h,** IPA analysis of *CDH18*-silenced d12 EPI cells (si18) versus control (scr) cells showing the activation pattern of signature genes involved in major important developmental pathways. **i,** Pathway enrichment analysis showing the proportional correlation of genes affected in important developmental pathways contributing to SMC differentiation.

[Analysis of Figure 4 was based on RNA-Seq dataset GSE165450].

Figure 5. *CDH18* is unable to block TGF-β-driven EMT towards SMC differentiation

a, Schematic illustration depicting the experimental workflow. **b**, Fluorescence microscopy pictures showing mCherry-expressing cells 3 days' post transfection (dpt) of d12 EPI cells [scale bar 100µm]. **c**, Flow cytometry analysis showing mCherry expression in EPI cells overexpressing *CDH18* 3 dpt [gating set using empty-transfected cells (Supplementary Figure 5b)]. **d-e**, Validation of ectopic *CDH18* cDNA overexpression demonstrating the increase of (**d**) *CDH18* by qRT-PCR and (**e**) CDH18 protein by western blot analysis upon plasmid transfection and sorting. **f**, Phase contrast pictures of un-/sorted *CDH18*-overexpressing cells induced towards iSMC (+TGF-β+bFGF) or cultured in EPI maintaining conditions (+SB4321542) [scale bar 100 µm]. **g-h**, Expression of (**g**) *CDH18* and (**h**) *ACTA2* in un-/sorted *CDH18*-overexpressing cells and control cells under both EPI maintaining (+SB4321542) and iSMC inducing (+TGF-β+ bFGF) culture conditions. **i**, Expression analysis based on RNA-Seq dataset [GSE165450] of selected SMC marker genes. **j**, Boyden chamber assay evaluating cell migration capacity in d12•si18 cells [n=3; paired students t-test; * p=0.0336, ** p<0.0054].
[unsorted transfected cells (OE), empty-transfected cells (neg), sorted mCherry-expressing cells (mCherry+), sorted non-mCherry-expressing cells (mCherry-); Statistical analysis performed by Repeated measure (RM) one-way ANOVA unless indicated otherwise: **** p<0.0001, *** p<0.0005, ** p<0.005, * p<0.05; all error bars represent SEM].

Figure 6. *CDH18* expression is under the control of *GATA4*

a, Venn diagram depicting the interface of positively correlative genes to *CDH18* (R ≥ 0.6) (light orange) and DEGs between early (Epi12) and late (Epi48) stage epicardium (target) (light brown) [GSE84085] revealed a total of 522 genes within their intersection. **b**, Classification of 23 transcription factors (TFs) by overlapping the list of TFs (bright green) and genes identified in (**a**) (grey). **c**, Binding site analysis showing the predicted binding sequence of *GATA4* and relative binding score. **d**, Co-expression network analysis of the qRT-PCR data of *GATA4* (Supplementary Figure 6c) and *CDH18* (Figure 2f) expression in EPI cells over time. **e-f,** Silencing of *GATA4* in d5 cells using two different siRNAs (siGata4#1 and siGata4#2) [n=3] shows (**e**) a reduction in epicardial cell density after 3 and 7 days and (**f**) the expression levels of *GATA4* and *CDH18* after 7 days [ns = not significant]. **g-h**, Silencing of *GATA4* in d12 cells using two different siRNAs (siGata4#1 and siGata4#2) [n=3] shows (**g**) morphological changes (blue arrowheads) after 3 and 7 days and (**h**) reduction of *GATA4* and *CDH18* expression, as revealed by qRT-PCR [*** $p<0.0005$, **** $p<0.0001$], as well as (**i**) loss of GATA4 and CDH18 protein expression, as shown by western blot analysis.

[statistical analysis performed by one-way ANOVA with Dunnett's multiple comparison test unless indicated otherwise. All error bars represent SEM; scale bars 100µm].

Supplementary Figure 1

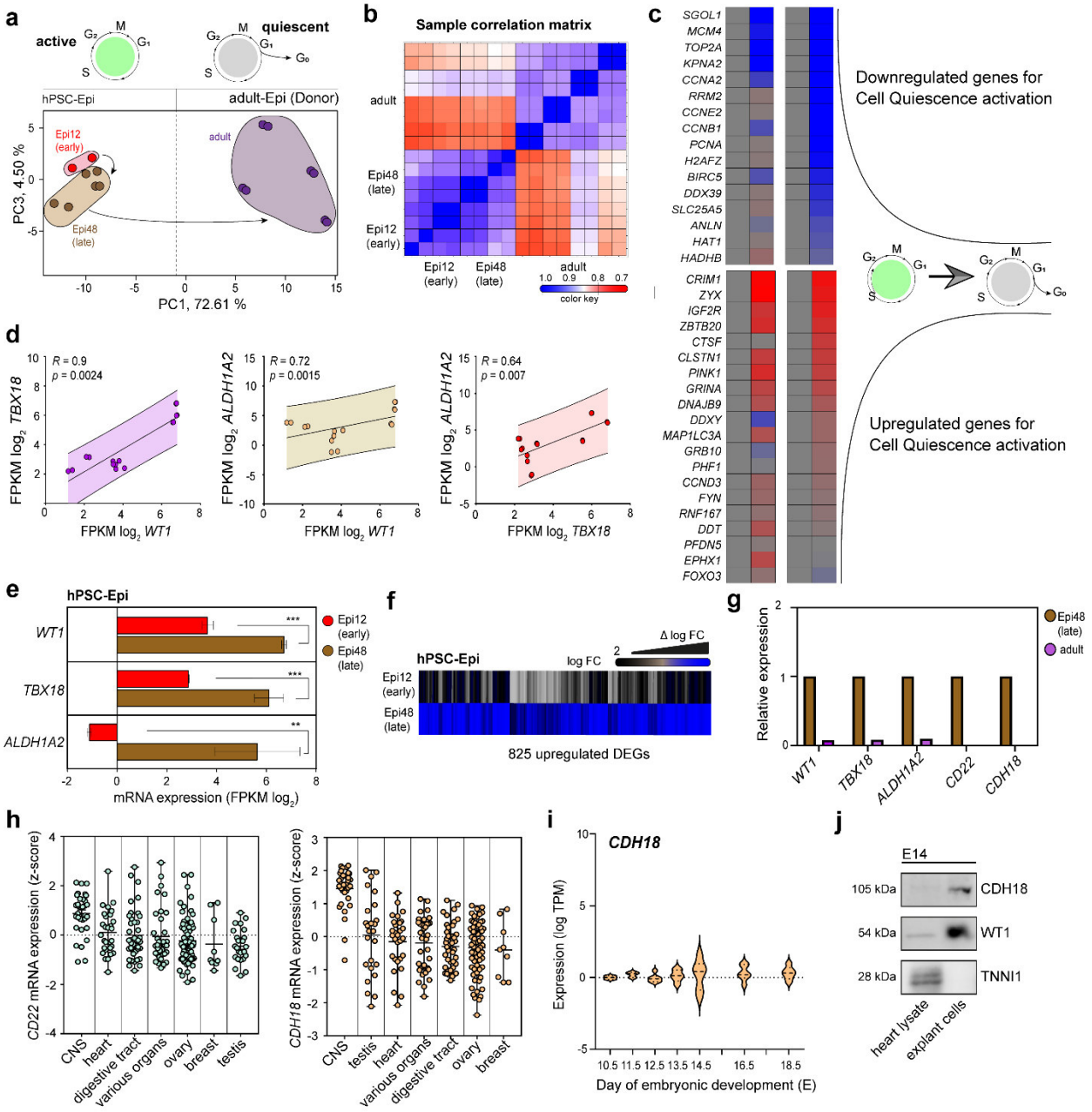

Supplementary Figure 1. Transcriptional profiling of active epicardial cells for cell surface markers

a PCA using the GSE84085 RNA-Seq expression dataset of d12 early epicardial-like cells (Epi12, red) [19-9-7-Epi, *n*=2], d48 late epicardial-like cells (Epi48, brown) [H9-Epi, ES03-Epi and 19-9-11-Epi, *n*=6] and human adult epicardium (dark violet) [donors 9605, 9633, 9634 and 9635, *n*=8]. **b,** Sample correlation matrix resulting from the consensus clustering analysis of mRNA data, shows transcriptomic differences among samples. **c,** Retrospective analysis showing a heatmap of quiescence marker genes in adult epicardium (adult) compared to embryonic induced epicardial cells Epi12 (right) and Epi48 (left). **d,** Transcriptomic correlative analysis (Pearson, R) of genes defining the embryonic epicardium. **e,** Analysis of *WT1*, *TBX18* and *ALDH1A2* expression Epi12 (red) and Epi48 (brown) [* $p<0.05$; ** $p<0.01$; *** $p<0.001$, students' t test]. **f,** DEG analysis to identify genes that are at least 2-fold upregulated in the active epicardium. **g,** Fold change of active epicardium markers and identified candidates in adult tissue (dark purple)

relative to Epi48 (brown). **h,** Ranked *CD22* (left) and *CDH18* (right) expression by tissue (z-score) [GSE7307]. **i**, GSE1479 retrospective analysis for *CDH18* mRNA expression in mouse heart embryonic development [*n*=36; E10.5 = 3, E11.5 = 3, E12.5 = 6, E13.5 = 6, E14.5 = 6, E16.5 = 6, E18.5 = 6] [One-way ANOVA]. **j**, Western blot analysis of CDH18, WT1 and cardiac troponin 1 (TNNI1) expression in murine fetal whole-heart lysate and fetal heart explant culture. [data shows GSE84085 unless stated otherwise]

Supplementary Figure 2

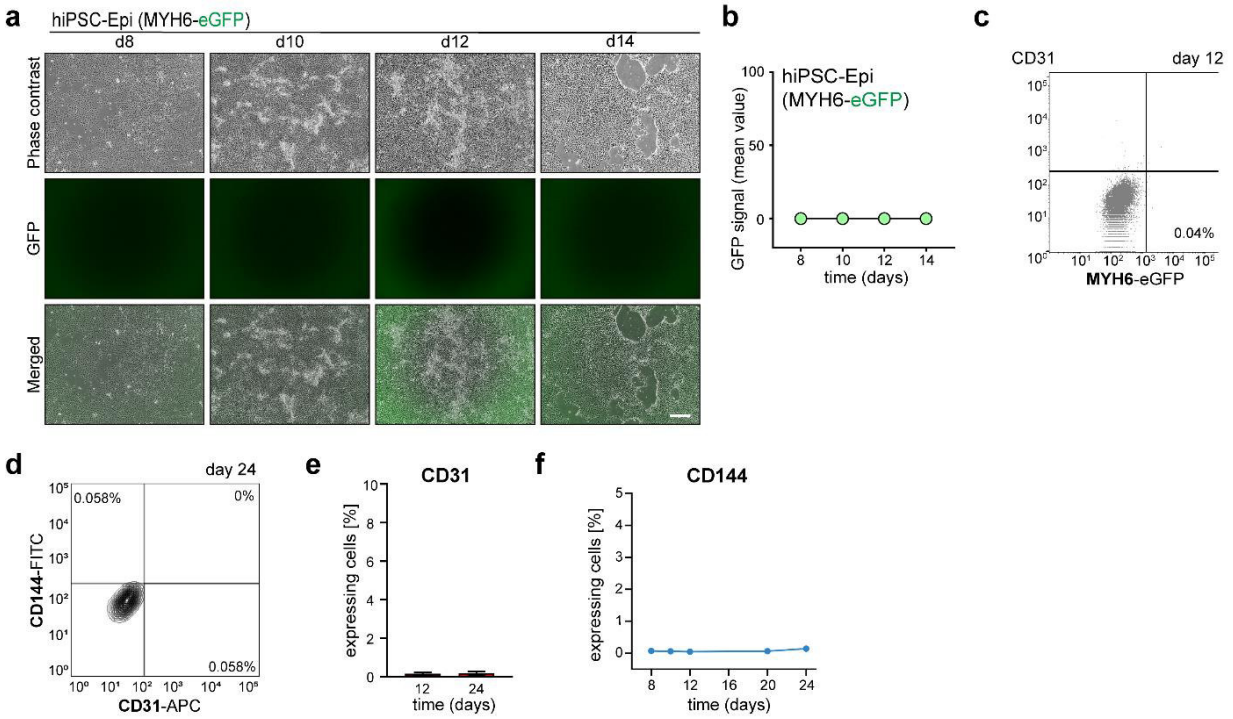

Supplementary Figure 2. Exclusion of cardiomyocyte traces

a, Phase contrast and fluorescent microscopy of EPI cells induced from MYH6-eGFP reporter line at d8-14 showing no visible eGFP expression [scale bar 200µm]. **b, c**, Flow cytometry analysis of **b** eGFP expression over time and **c** CD31 and eGFP expression in d12 EPI cells [*n*=3]. **d-f**, Detection of CD31 and CD144: **d** contour blot of d24 EPI cells; **e** CD31 expression in d12 and d24 EPI cells and **f** CD144 expression over time of induction.

Supplementary Figure 3

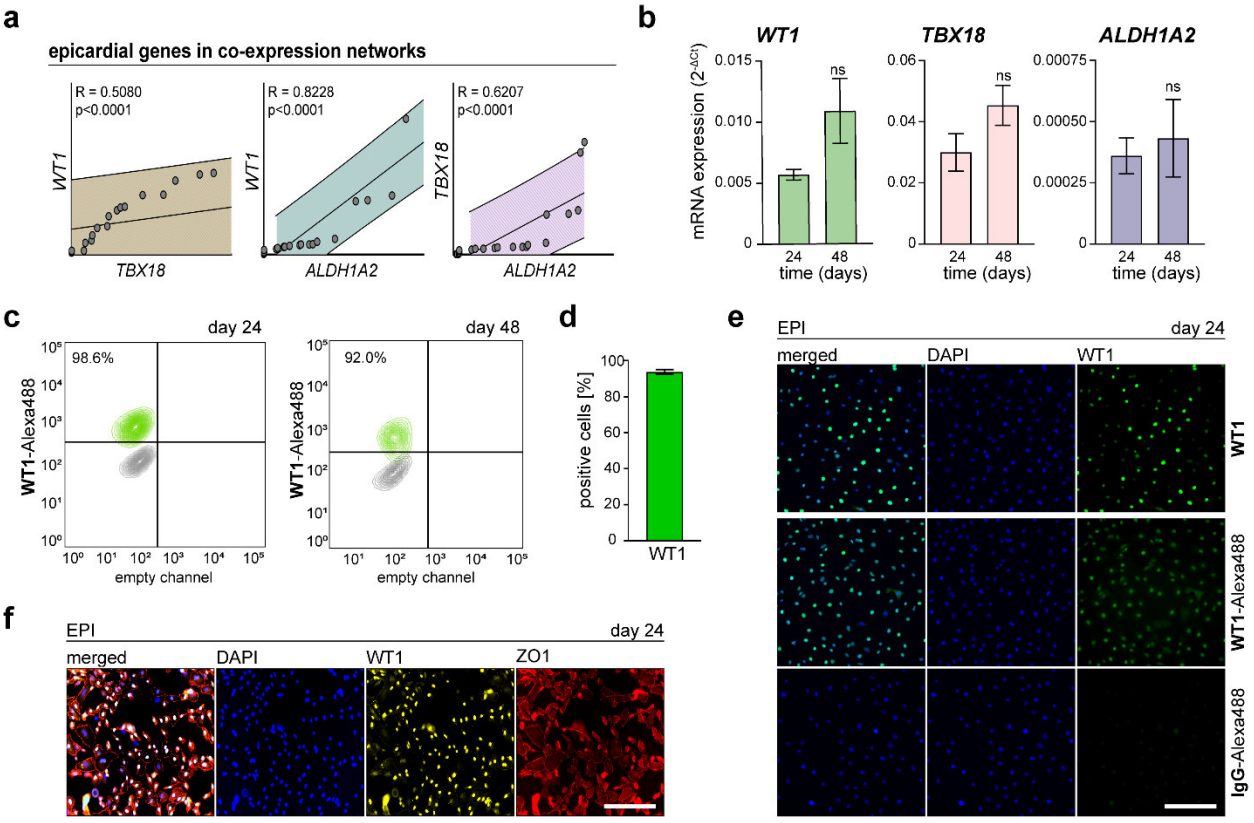

Supplementary Figure 3. Molecular characterization of EPI cells

a, Transcriptomic correlative analysis (Pearson, R) of genes defining the fetal stage of epicardial development in EPI cells based on (Fig. 2c). **b**, qRT-PCR analysis of epicardial markers *WT1* (light green), *TBX18* (light red) [d24 *n*=8, d48 *n*=10] and *ALDH1A2* (light purple) [d24, d48 *n*=8]. There was no statistically significant difference (ns) between d24 and d48 [Mann-Whitney-test; error bars indicate standard error of the mean (SEM)]. **c**, Flow cytometry-derived contour blot of d24 (left) and d48 (right) EPI cells showing WT1 expression (green) [gray, unstained control]. **d-f**, EPI d24 cells showing WT1 expression and **d** its quantification of positive cells counted in ImageJ. **e,** Immunofluorescence staining of cells was performed using both purified and conjugated WT1 antibody to confirm positivity of cells. **f,** EPI cells display cobblestone-like cell morphology and the expression of ZO1 and WT1. DAPI staining marks cell nuclei [scale bar 100µm; images were cropped to show a representative section].

Supplementary Figure 4

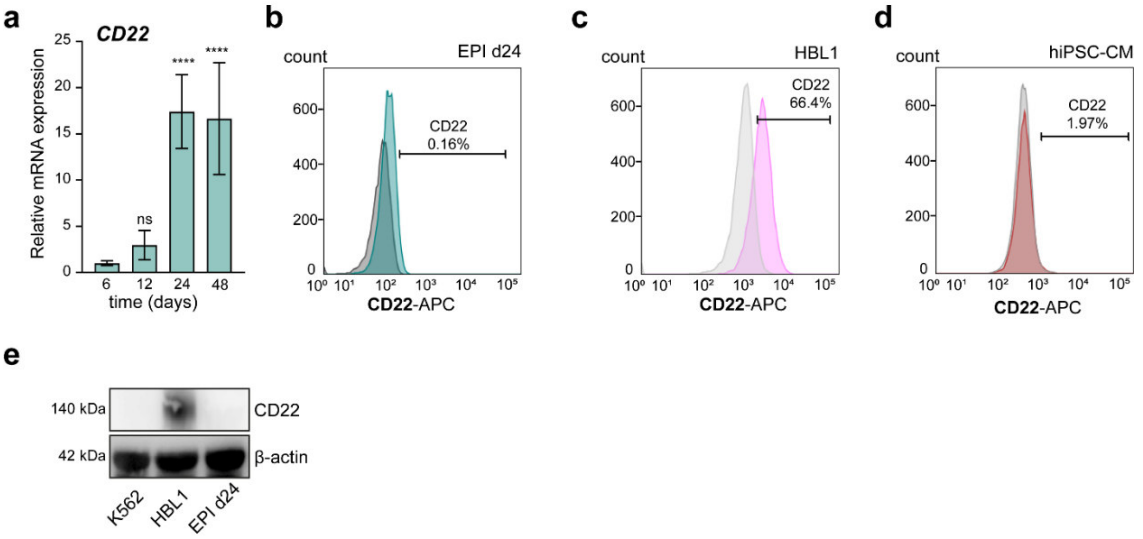

Supplementary Figure 4. Evaluation of CD22 expression

a, qRT-PCR analysis of *CD22* (deep turquoise) during induction normalized to d6. [d6 *n*=4, d12 *n*=4, d24 *n*=8, d48 *n*=8; **** $p<0.0001$]. **b**, Flow cytometry analysis for CD22 (deep turquoise) [gray, unstained control]. **c,d**, Flow cytometry analysis for CD22 in **c** HBL1 cells (light pink) acting as a positive control and **d** hiPSC-derived CM (hiPSC-CM) (dark red) acting as a negative control [grey, unstained control]. **e**, Western blot analysis for CD22 in EPI cells at d24 with HBL1 cells acting as a positive control and K562 cells acting as a negative control.

Supplementary Figure 5

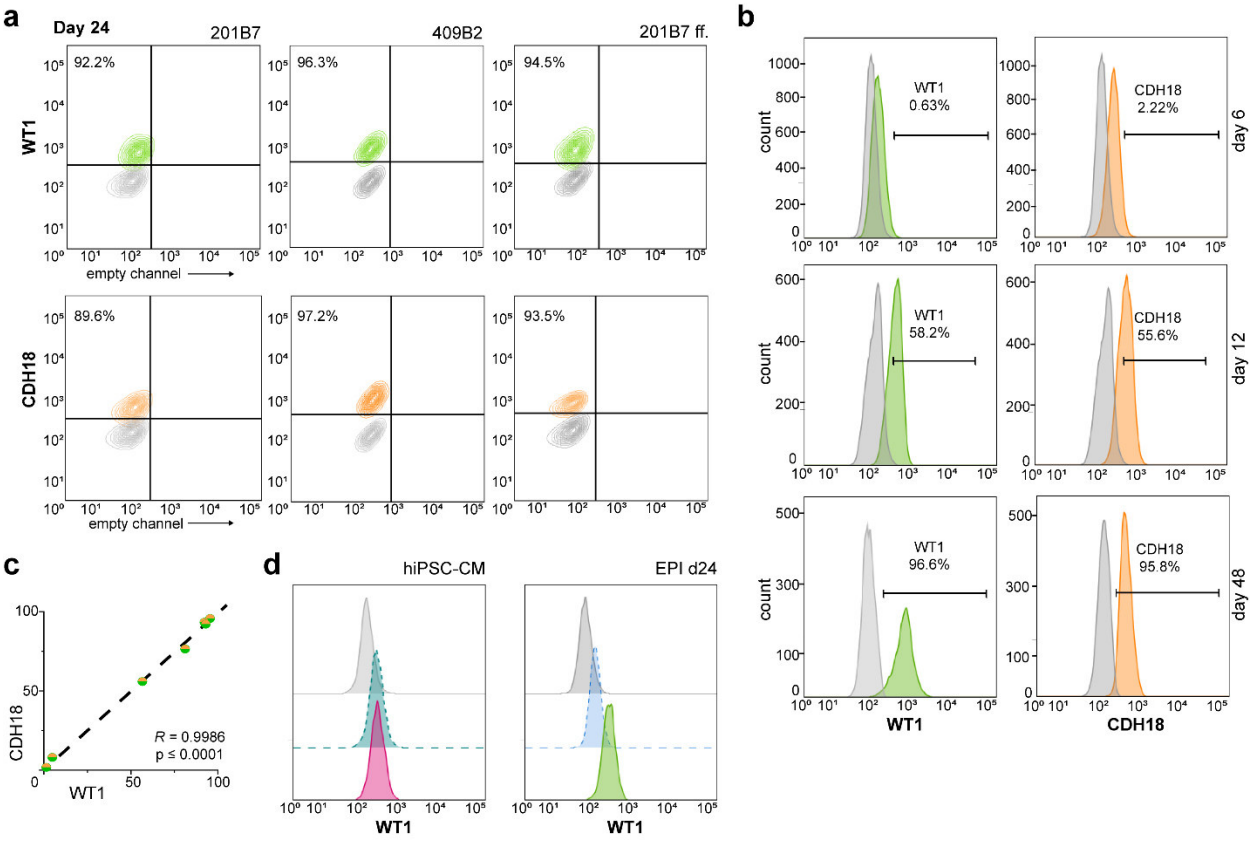

Supplementary Figure 5. Evaluation CDH18 as a putative biomarker in epicardiogenesis

a, Contour blots of d24 EPI cells showing WT1 (upper panel, green) and CDH18 (lower panel, orange) expression in cells differentiated from 201B7 and 409B2 maintained on-feeder and 201B7 maintained feeder-free (ff.). **b**, Histograms depicting WT1 (left, green) and CDH18 (right, orange) expressions detected by flow cytometry in d6, d12 and d48 EPI cells. **c**, Correlation analysis (data Fig. 2h) for WT1 and CDH18 expression. **d**, Half-Offset overlay histograms of WT1 expression in hiPSC-CM (dark pink) showing no WT1 expression and EPI cells at d24 (green) [dotted lines mark isotype control, turquoise: hiPSC-CM; light blue: EPI; gray: unstained cells].

Supplementary Figure 6

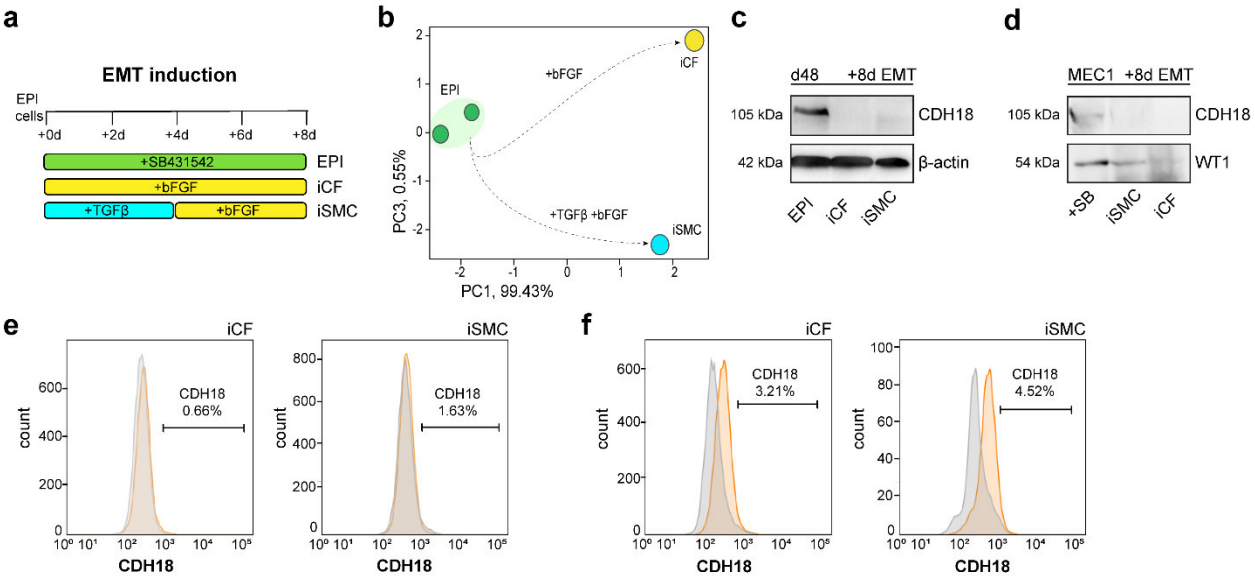

Supplementary Figure 6. CDH18 expression in EPDCs

a, Scheme of EMT induction for the directed differentiation of induced CF (iCF) and induced SMC (iSMC). **b**, PCA plot of EPI cells at d24, induced CF (iCF) and SMC (iSMC) [GSE165450]. **c**, Western blot analysis for CDH18 expression in EPI cells and derivatives derived from d48. **d**, CDH18 and WT1 expression analysis in MEC1 cell line treated accordingly to EMT induction scheme described in **a** [+SB = +SB431542]. **e, f**, Histogram showing CDH18 expression in EPDCs derived from **e** d12 and **f** d24 EPI cells.

Supplementary Figure 7

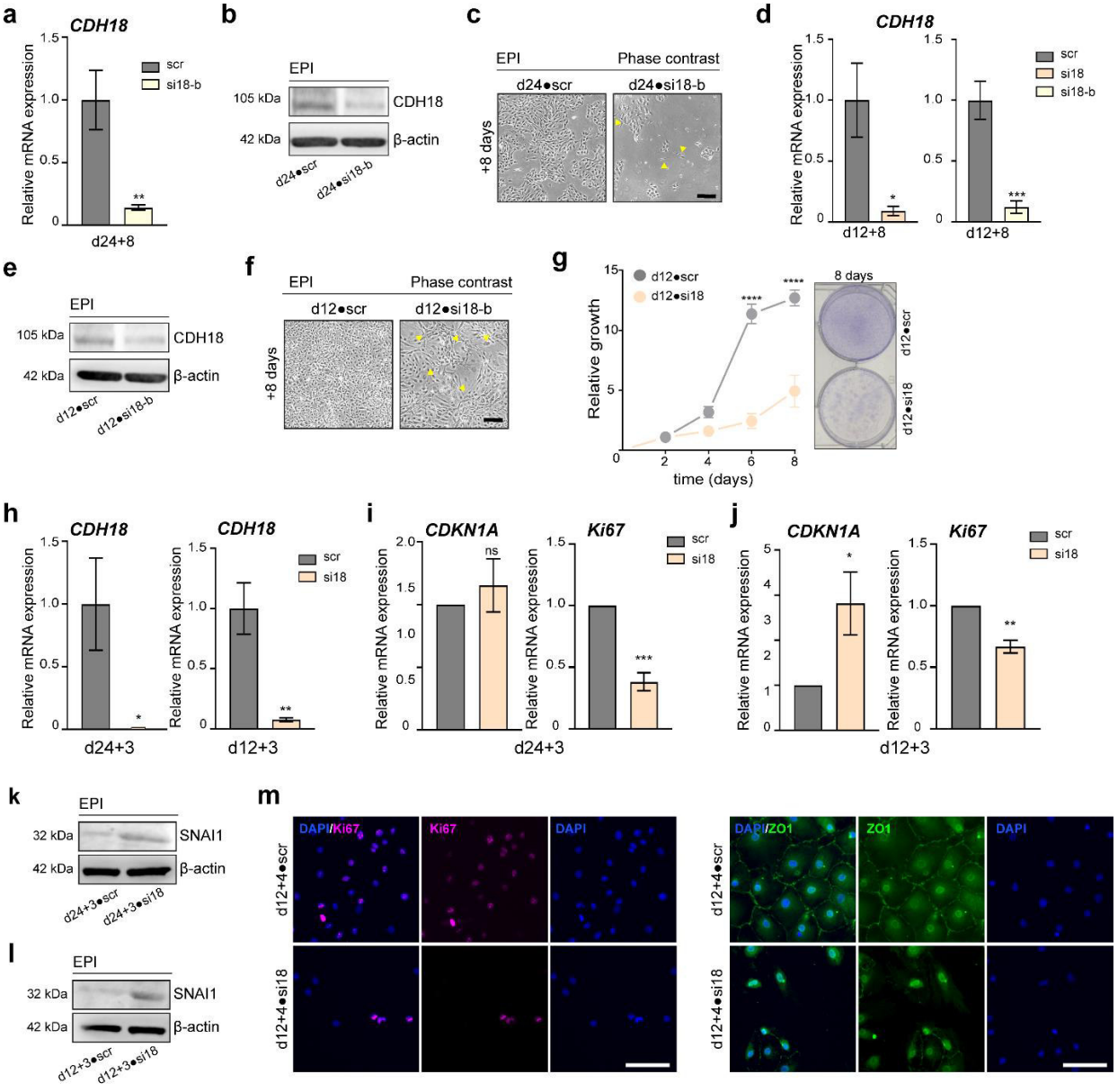

Supplementary Figure 7. Downregulation of *CDH18* leads to loss of epicardial identity and initiation of EMT

a-c, *CDH18* downregulation by a second siRNA against *CDH18* (si18-b) in d24 EPI cells: **a** Reduction of mRNA expression [*n*=3; ** *p*=0.0048] and **b** protein expression and **c** changed morphology, i.e., elongated cells (yellow arrowheads). **d**, Knockdown verification 8 days after silencing using two different siRNAs against *CDH18* in d12 EPI cells [*n*=3; * *p*=0.014, *** *p*=0.0003]. **e, f**, Validation of **e** reduced CDH18 and **f** changes morphology (yellow arrowheads) in si18-b-treated cells after 8 days. **g**, Growth curve of d12 cells silenced for *CDH18* and control (scr) for 2-8 days [*n*=3; **** *p*<0.0001]. **h**, Knockdown verification 3 days after silencing of *CDH18* in d24 (left) and d12 (right) EPI cells [*n*=3; * *p*=0.0222, ** *p*=0.0016]. **i, j**, Downregulation of proliferation markers 3 days after silencing in **i** d24 and **j** d12 EPI cells [scr normalized to 1 for each experiment; *n*=3; paired Students t-test: * *p*=0.0483, ** *p*=0.0013, *** *p*=0.0004, ns= not significant]. **k, l**, Western blot analysis for SNAI1 detection

upon 3 days after silencing in **k** d24 and **l** d12 EPI cells. **m**, Immunofluorescence staining of d12 EPI cells 4 days after silencing for Ki67 and ZO1 expression. [scale bars = 100µm; statistical analysis performed by Students t-test unless indicated otherwise, error bars represent SEM].

Supplementary Figure 8

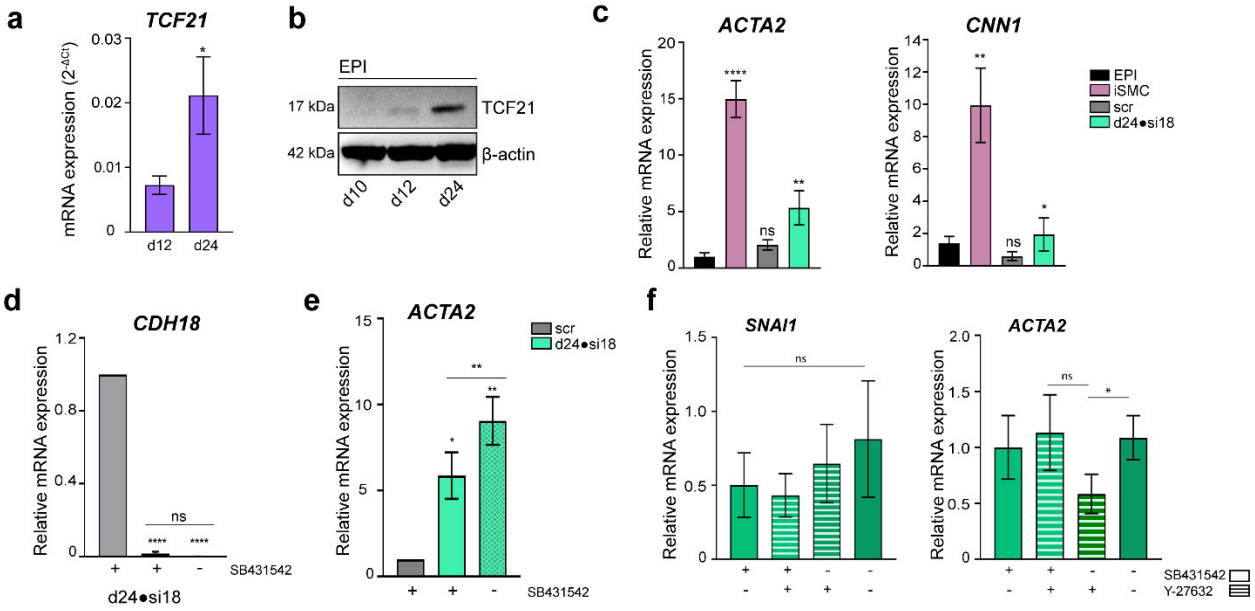

Supplementary Figure 8. Downregulation of *CDH18* induced differentiation into SMC

a, b, Expression levels for *TCF21* from d12 to d24 based on **a** qRT-PCR [*n*=4] and **b** western blot analysis. **c**, Expression of SMC markers in d24 EPI cells either silenced (si18) or induced towards SMC (iSMC) for 8 days. Cells displayed an upregulation of *ACTA2* (left) and *CNN1* (right) in both iSMCs and si18 cells but not in EPI or scr-treated cells, albeit upregulation in d24•si18 was only modest. Data is normalized to EPI cells [*n*=3; Students t-test: * $p<0.05$, ** $p<0.009$, *** $p<0.0005$, **** $p<0.0001$]. **d, e**, Expression of **d** *CDH18* and **e** *ACTA2* in d24 silenced cells in presence or absence of TGFβ-inhibitor (SB431542) [scr normalized to 1 for each experiment; *n*=3; RM-one-way ANOVA; * $p<0.05$, ** $p<0.009$, **** $p<0.000$]. **f**, Expression of *SNAI1* (left) and *ACTA2* (right) in d12 silenced cells in presence or absence of TGFβ-inhibitor (SB431542) and ROCK inhibitor (Y-27632) [*n*=3; RM-one-way ANOVA with Tukey's multiple comparison test; * $p<0.0367$]. [error bars indicate SEM].

Supplementary Figure 9

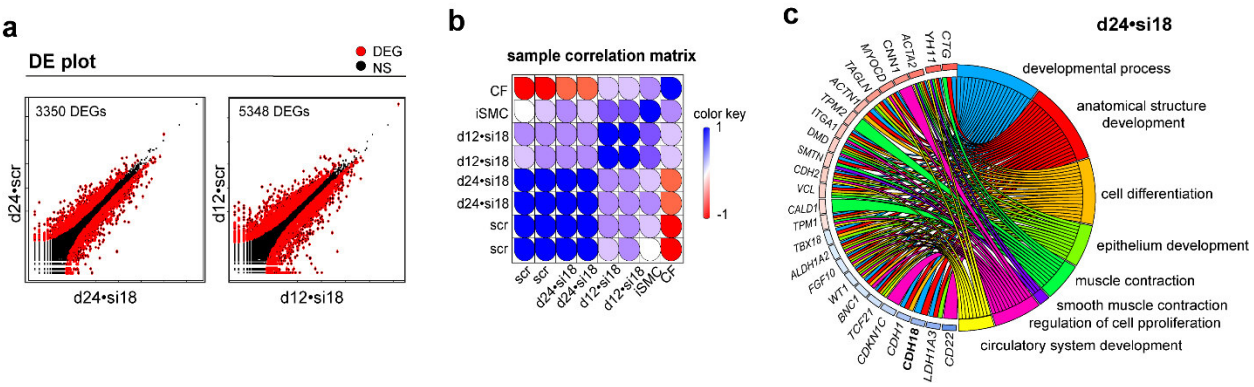

Supplementary Figure 9. Transcriptional profiling of *CDH18*-silenced EPI cells

a, Differential expression (DE) plot showing the number of DEGs (red dots) in *CDH18*-silenced d24 EPI (d24•si18, left) and d12 EPI (d12•si18, right) cells. Black dots indicate genes without significantly different expression (NS). **b**, Sample correlation matrix resulting from the consensus clustering analysis of mRNA data and showing transcriptomic differences among samples [GSE165450]. **c**, Chord diagram representing flow and detailed relationship between gene expression levels of d24•si18 DEGs (left semicircle perimeter) and their enriched GO biological processes (right semicircle perimeter) [GSE165450].

Supplementary Figure 10

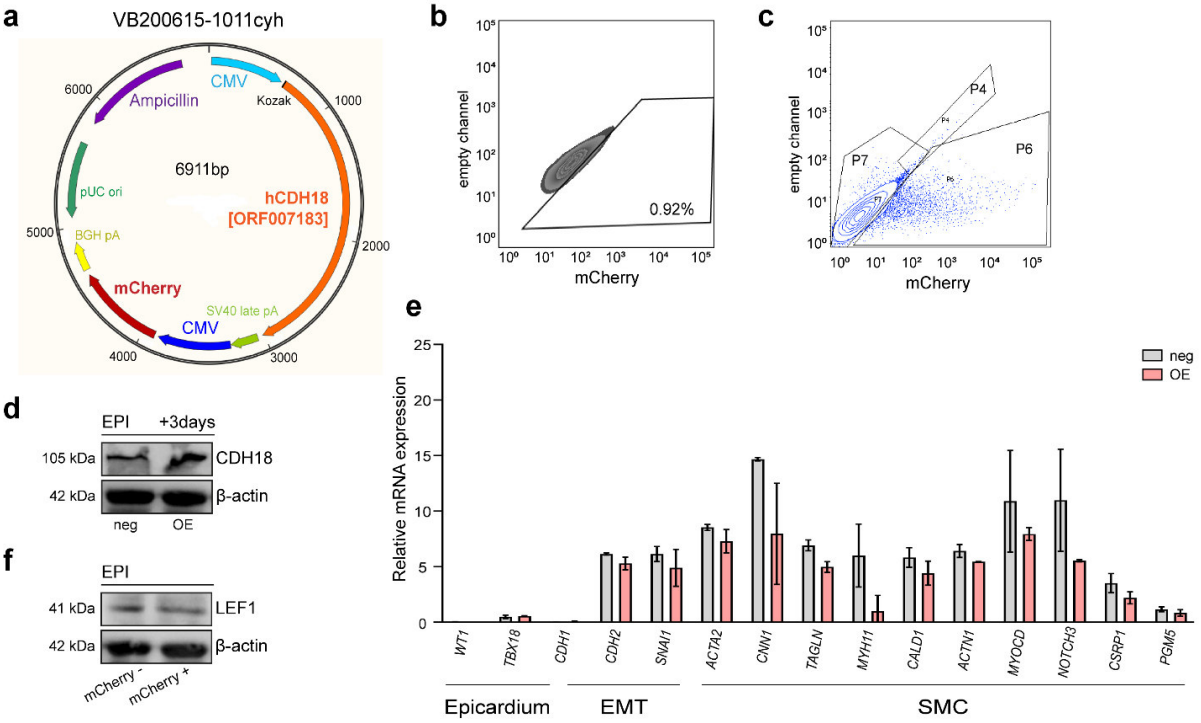

Supplementary Figure 10. *CDH18* overexpression in EPI cells

a, Vector map generated using SnapGene® of *CDH18* overexpression plasmid designed using the VectorBuilder platform [VB200615-1011cyh], containing human *CDH18* cDNA under a CMV promotor as well as mCherry-expression cassette for transfection validation. **b**, Flow cytometry analysis of non-mCherry expressing (mCherry-) cells. **c**, FACS gating: The P6 population was classified as mCherry+, P7 as mCherry-. The P4 population was defined as highly auto-fluorescent cells and therefore excluded from sorting. **d**, Knockdown verification 3 days after transfection in transfected (OE) and empty transfected (neg) cells. **e**, Expression analysis of RNA-seq dataset [GSE165450] of characteristic signature genes in OE and neg cells. **f**, LEF1 expression in mCherry + sorted and mCherry – sorted cells.

Supplementary Figure 11

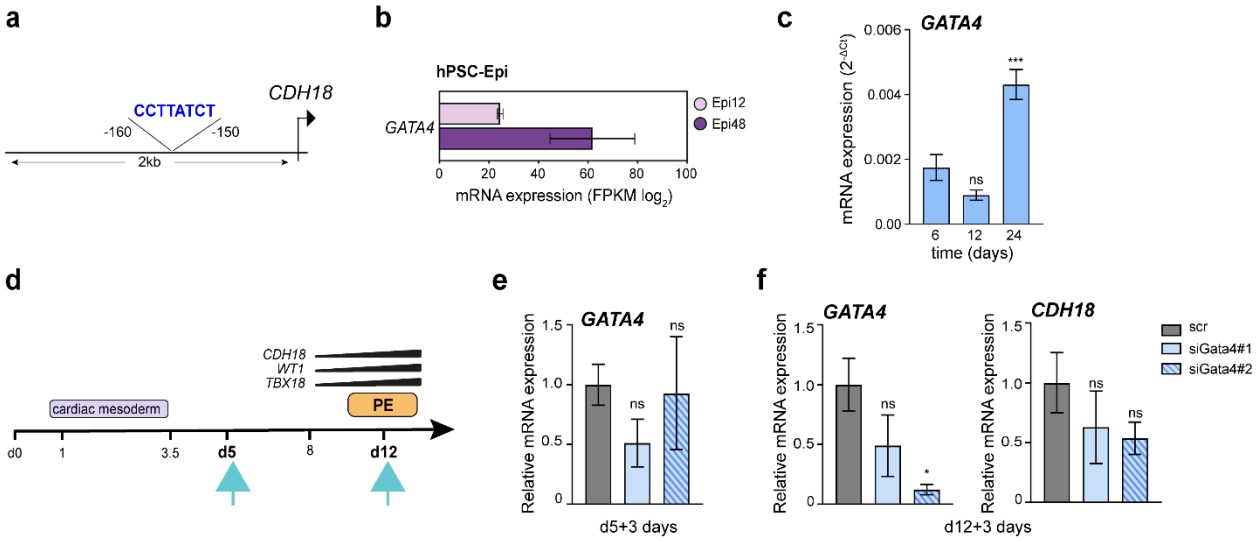

Supplementary Figure 11. Characterization of *GATA4* expression during epicardial formation

a, *CDH18* promotor region (2 kb) with the predicted binding sequence of *GATA4* identified by binding site analysis. **b**, *GATA4* expression in Epi12 and Epi48 cells [GSE84085]. **c**, Time course of *GATA4* expression during EPI induction analyzed by qRT-PCR [d6-12, *n*=4; d24 *n*=8; *** *p*=0.007]. **d**, Scheme of the silencing experiments during EPI induction. **e, f**, Day 3 after silencing using two different siRNAs (siGata4#1 and siGata4#2) in **e** d5 EPI cells showing *GATA4* expression and **f** d12 EPI cells showing *GATA4* and *CDH18* expression [*n*=3; ns (non-significant), * *p*<0.05]. [statistical analysis performed by one-way ANOVA with Dunnett's multiple comparison test; error bars represent SEM].

Supplementary Figure 12

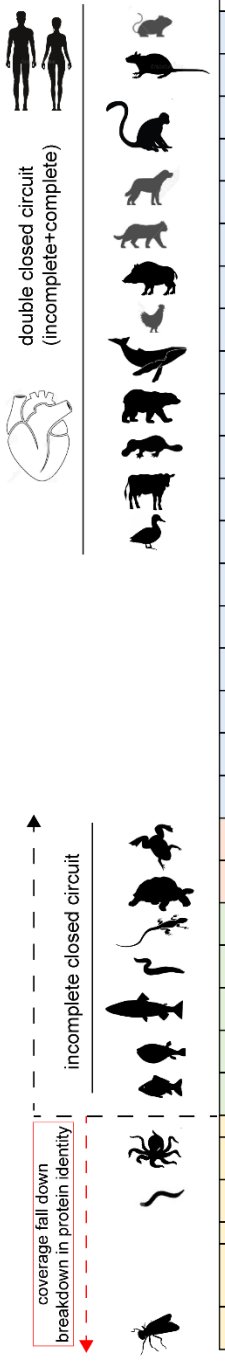

Organism	Protein name	Query coverage [%]	Identity [%]	Homo-/Orthologous	NCBI	Uniprot	Circulatory system
Mus musculus	cadherin-18 precursor	100	96.08	Yes/Yes	NP_001074768.1	E9Q9Q6	double closed
Rattus novergicus	cadherin-18 precursor	100	96.71	Yes/Yes	NP_001101126.2	F1M702	double closed
Pan troglodytes	cadherin-18 isoform X1	100	99.62	Yes/Yes	XP_024212431.1	H2QQP5	double closed
Pongo abelii	cadherin-18 isoform X1	100	99.37	Yes/Yes	XP_024103414.1	H2PF84*	double closed
Canis lupus familiaris	cadherin-18 isoform X1	100	97.22	Yes/Yes	XP_013968634.1	F6Y5X3	double closed
Felis catus	cadherin-18 isoform X4	100	97.22	Yes/Yes	XP_019668046.1	M3WJ78	double closed
Sus scrofa	Cadherin-18 isoform X1	100	97.59	Yes/Yes	XP_020932622.1	A0A287AN03	double closed
Gallus gallus	cadherin-18 isoform X4	100	91.77	Yes/Yes	XP_426046.4	A0A1D5PZT9	double closed
Balaenoptera acutorostrata scammoni	cadherin-18 isoform X1	100	96.58	Yes/Yes	XP_007188294.1	A0A384ALT3_BALAS	double closed
Ursus maritimus	cadherin-18 (predicted)	100	96.96	Yes/Yes	XP_008688109.1	A0A384C0Z5	double closed
Ornithorhynchus anatinus	cadherin-18	100	89.57	Yes/Yes	XP_001507828.2	F6VFP8	double closed
Bos taurus	cadherin-18 precursor	100	97.08	Yes/Yes	NP_001070305.1	Q08DJ5	double closed
Anas platyrhynchos	Cadherin-18	100	91.37	Yes/Yes	EOA99298.1	A0A493U2B5	double closed
Callorhinchus mili	Cadherin-18 (predicted)	100	75.06	Yes/Yes	XP_007899915.1	A0A4W3IDI2	double closed
Aquila chrysaetos chrysaetos	cadherin-18 isoform X2	100	91.39	Yes/Yes	XP_029897709.1	A0A663FAS0	double closed
Gallus gallus	cadherin-18 isoform X4	100	91.77	Yes/Yes	XP_426046.4	A0A1D5PZT9	double closed
Balaenoptera acutorostrata scammoni	cadherin-18 isoform X1	100	96.58	Yes/Yes	XP_007188294.1	A0A384ALT3_BALAS	double closed
Ursus maritimus	cadherin-18 (predicted)	100	96.96	Yes/Yes	XP_008688109.1	A0A384C0Z5	double closed
Ornithorhynchus anatinus	cadherin-18	100	89.57	Yes/Yes	XP_001507828.2	F6VFP8	double closed
Xenopus laevis	cadherin-18-like isoform X2 (predicted)	100	83.8	Yes/Yes	XP_018124907.1	A0A1L8FS65	incomplete closed
Terrapene carolina triunguis	Cadherin-18	100	62.12	Yes/No	XP_029768360.1	A0A674JC42	incomplete closed
Anolis carolinensis	cadherin-18 isoform X1 (predicted)	100	90.76	Yes/Yes	XP_008112423.1	H9GMS7	incomplete closed
Mastacembelus armatus	cadherin-18-like isoform X1	100	75.88	Yes/Yes	XP_026147849.1	A0A3Q3MBN2	incomplete closed
Salmo trutta	cadherin-18-like (uncharacterized)	99	74.24	Yes/Yes	XP_029612053.1	A0A673X3T7	incomplete closed
Takifugu rubripes	cadherin-18	100	73.87	Yes/Yes	XP_003968224.1	A0A674MQU2	incomplete closed
Lates calcarifer	cadherin-18 (predicted)	100	75	Yes/Yes	XP_018534785.1	A0A4W6G877	incomplete closed
Loligo vulgaris	No results						
Octopus vulgaris	protocadherin Fat 1-like isoform X3	67	32.46	No/No	XP_029644443.1	-	closed
Caenorhabditis elegans	protocadherin Fat 1-like isoform X3	67	30.66	No/No	NP_506256.3	G5EDK5	none
Lumbricus terrestris	No results						
Apis mellifera	fat-like cadherin-related tumor suppressor homolog isoform X9	71	33.98	No/No	XP_026296988.1	-	open
Drosophila melanogaster	Cadherin-N, isoform L	83	30.37	No/No	NP_001027277.1	Q4ABE7	open

Supplementary Figure 12. CDH18 protein conservation and cardiovascular development

Phylogenetic analysis of the CDH18 protein sequence in cardiovascular double-circuit, incomplete closed circuit and open circuit species.

Supplementary Figure 13

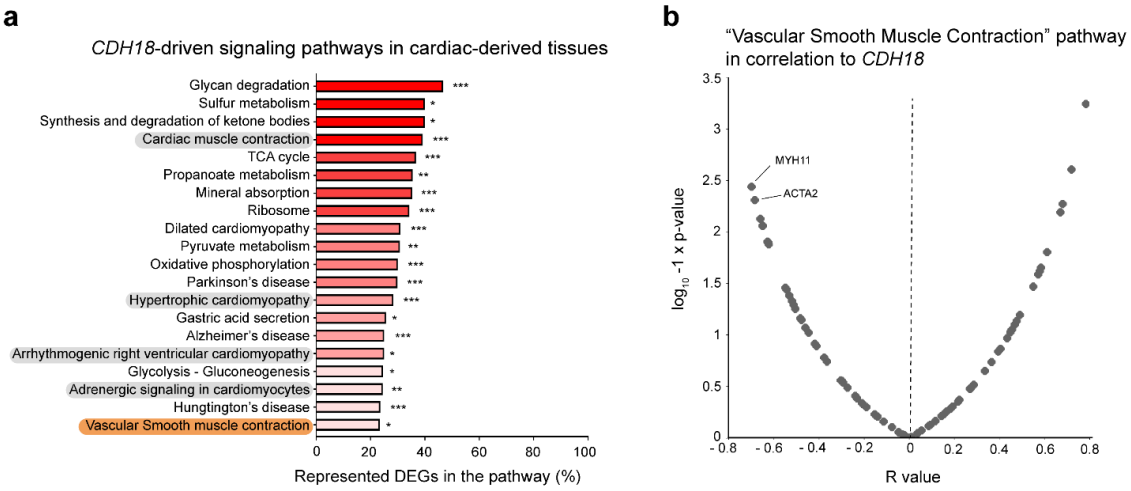

Supplementary Figure 13. CDH18 related signaling pathways

a, KEGG pathway activity correlation pattern analysis for *CDH18* expression in cardiovascular system-derived tissues [GSE7307; aorta, coronary-artery, heart, heart atrium, heart ventricle; total *n*=15; Pearson R; * $p<0.05$, ** $p<0.01$, *** $p<0.001$]. **b**, Volcano plot analysis for genes in cardiovascular system-derived tissues in correlation to *CDH18* [GSE7307; aorta, coronary-artery, heart, heart atrium, heart ventricle; total *n*=15].

Supplementary Table 1a: Optimization of transfection time

FuGENE®HD: 3µg plasmid/6-well	2:1	3:1	4:1
+24h (ST)	3.95%	2.57%	2.42%
+48h (ST)	**12.50%**	8.00%	7.00%
+48h (RT)	11.70% *		

Supplementary Table 1b: Optimization of transfection agent

Transfection reagent 2:6µg plasmid/6-well	FuGENE®HD	FuGENE®6	PEI	Lipofectamine™ 3000
+48h (ST)	14.60%	18.20%	4.38%	
+72h (ST)	14.70%	**24.60%**		28.80% *
+72h (RT)		13.30%		

Supplementary Table 1. Optimization of transfection protocol

a, b, Optimization of the transfection protocol showing percentage of mCherry+ cells. The left column shows the time after the transfection using either the standard transfection (ST) or reverse transfection (RT) method. **a** 3µg plasmid DNA per one well of a 6-well-plate and FuGENE®HD transfection reagent was used to assess different transfection agent-to-DNA ratios (upper column). **b** 6 µg plasmid DNA per one well of a 6-well-plate was used to assess different transfection agents (upper column). Albeit transfection efficiency with Lipofectamine 3000 was higher, due to high cell toxicity the total amount of mCherry+ sorted cells was low. [* indicates conditions with low cell survival, bold marked values indicate highest absolute amount of transfected cells]

Supplementary Table 2.

Genes	Sequences (5' – 3')
WT1	**F:** ATAGGCCAGGGCATGTGTATGTGT **R:** AGTTGCCTGGCAGAACTACATCCT
TBX18	**F:** TTAACCTTGTCCGTCTGCCTGAGT **R:** GTAATGGGCTTTGGCCTTTGCACT
ALDH1A2	**F:** TTTGCCAAGTTCCATTGTGCCAGG **R:** TGGTGGAGTCACTGGAAAGCAGAA
CD22	**F:** GGTCAGCCTCCAATGTGACT **R:** CTGGCTCTGTGTCCTCTTCC
CDH18	**F:** AATGACAATCCACCCGAAC **R:** GGCTGTGTTATCTTCATTGTCC
CDH1	**F:** TTCTGCTGCTCTTGCTGTTT **R:** TGGCTCAAGTCAAAGTCCTG
CDH2	**F:** CTCCAATCAACTTGCCAGAA **R:** ATACCAGTTGGAGGCTGGTC
ACTA2	**F:** TCAATGTCCCAGCCATGTAT **R:** CAGCACGATGCCAGTTGT
CNN1	**F:** AAGGACGCACTGAGCAACGCTATT **R:** ACGCCACTGTCACATCCACATAGT
GAPDH	**F:** TGATGACATCAAGAAGGTGGTGAAG **R:** TCCTTGGAGGCCATGTGGGCCAT
TCF21	**F:** AGGCAGATCCTGGCTAACGACAAA **R:** TCCAGGTACCAAACTCCAAGGTCA
GATA4	**F:** TTCCAGCAACTCCAGCAACG **R:** GCTGCTGTGCCCGTAGTGAG

Supplementary Table 2. List of qRT-PCR primers